

Kernel Two-Sample Tests for Manifold Data

Xiuyuan Cheng* Yao Xie†

Abstract

We present a study of kernel based two-sample test statistic, which is related to the Maximum Mean Discrepancy (MMD), in the manifold data setting, assuming that high-dimensional observations are close to a low-dimensional manifold. We characterize the test level and power in relation to the kernel bandwidth, the number of samples, and the intrinsic dimensionality of the manifold. Specifically, we show that when data densities are supported on a d -dimensional sub-manifold \mathcal{M} embedded in an m -dimensional space, the kernel two-sample test for data sampled from a pair of distributions (p, q) that are Hölder with order β is consistent and powerful when the number of samples n is greater than $\delta_2(p, q)^{-2-d/\beta}$ up to certain constant, where δ_2 is the squared ℓ_2 -divergence between two distributions on manifold. Moreover, to achieve testing consistency under this scaling of n , our theory suggests that the kernel bandwidth γ scales with $n^{-1/(d+2\beta)}$. These results indicate that the kernel two-sample test does not have a curse-of-dimensionality when the data lie on a low-dimensional manifold. We demonstrate the validity of our theory and the property of the kernel test for manifold data using several numerical experiments.

1 Introduction

Two-sample testing, aiming to determine whether two collections of samples are from the same distribution, is one of the fundamental problems in statistics and signal processing with a wide range of applications in scientific discovery and machine learning areas. Some examples include anomaly detection [11, 12, 6], change-point detection [56, 10, 55], single-cell data differential analysis [58], model criticism [36, 16, 7], general data analysis of biomedical data, audio and imaging data [8, 17, 31, 14], as well as machine learning applications [34, 37, 51, 16, 32, 38]. In the classical setting, given two independent sets of data in \mathbb{R}^m ,

$$x_i \sim p, i = 1, \dots, n_X, \text{ i.i.d.}, \quad y_j \sim q, j = 1, \dots, n_Y, \text{ i.i.d.}, \quad (1)$$

the two-sample problem seeks to accept or reject the null hypothesis $H_0 : p = q$. In (1), we assume that the data follow distributions with densities p and q respectively. It is also of application interest to identify where $p \neq q$ when the two distributions differ.

Traditional statistical methods for two-sample tests have been focusing on the parametric or low-dimensional testing scenarios, such as Hotelling’s two-sample test [29] and Student’s t-test [42]. When it is difficult to specify the exact parametric form of the distributions, non-parametric two-sample tests are more appropriate. Earlier works for one-dimensional non-parametric two-sample tests are based on the Kolmogorov-Smirnov distance [43, 33], the total variation distance [24], among others. Extension of these tests to high dimensional data is non-trivial. Modern non-parametric tests for high-dimensional data have been developed and many are based on the integral probability metrics [50]. A notable contribution is the Reproducing Kernel Hilbert Space (RKHS) Maximum Mean Discrepancy (MMD) two-sample test [20,

*Department of Mathematics, Duke University. Email: xiuyuan.cheng@duke.edu

†H. Milton Stewart School of Industrial and Systems Engineering, Georgia Institute of Technology. Email: yao.xie@isye.gatech.edu.

22, 23], which is related to U-statistics [47]. The asymptotic optimality of kernel based tests was recently studied in [2, 35]. Wasserstein distance two-sample test has been considered in [19, 44]; Graph-based statistics have been proposed for distribution-free tests in high dimension [13, 5]. However, it is known that non-parametric two-sample tests face difficulties for high-dimensional data, since the sample complexity for estimating those distance functions suffers from the curse-of-dimensionality. For instance, as pointed out in [45], the power of kernel based tests decreases polynomially with an increasing dimension of distributions.

The manifold data setting in this paper assumes that p and q are supported on (or near to) a d -dimensional manifold \mathcal{M} embedded in \mathbb{R}^m , $d \leq m$. We call \mathbb{R}^m the ambient space, and d the intrinsic dimensionality of the manifold data. The manifold data assumption naturally arises in applications, including image data [9, 41], biological data such as single-cell RNA sequencing data [25, 39], as well as features extracted by deep neural networks [46, 59]. In the geometrical data analysis and manifold learning literature, seminar works [3, 4, 26, 18] show that the graph diffusion process on a kernelized affinity graph constructed from such high-dimensional data vectors converges to a continuous diffusion process on the manifold, as the sample size increases to infinity and the kernel bandwidth decreases to zero. [49] and follow-up works show the approximation error to the manifold diffusion operator at a finite sample size, where the sampling complexity only involves the intrinsic dimensionality d . In the context of kernel density estimation (KDE), [40] shows that for data distribution lying on a submanifold embedded in the high-dimensional space, the convergence rate of the kernel density estimation only depends on the intrinsic dimensionality of the submanifold.

In the kernel MMD literature, the roles of the kernel bandwidth and the data dimensionality were not explicitly specified in the original kernel MMD paper [21]. For kernel MMD in high dimension, [45] provided a negative result that the test power decreases when applying to detect the mean shift of high-dimensional Gaussian distributions as the dimension increases. However, the argument therein does not consider possible intrinsically low-dimensional structures of high dimensional data. Thus the following questions remain unclear:

Question 1. *Will the similar effect – decreasing test power for an increasing data dimension – exhibit when the data have an intrinsically low-dimensional structure such as embedded sub-manifolds?*

Question 2. *When applying kernel tests to manifold data, how to choose the kernel bandwidth, which usually significantly influences the performance of kernel methods?*

The current paper provides a positive answer to Question 1 by providing a non-asymptotic result. Theoretically, we show that when data densities are supported on a d -dimensional sub-manifold \mathcal{M} embedded in \mathbb{R}^m (means manifold data with no noise), the kernel two-sample test is consistent and powerful when the number of samples n is greater than $\delta_2(p, q)^{-2-d/\beta}$ up to a certain constant, where δ_2 is the squared ℓ_2 -divergence between two distributions on manifold. Meanwhile, to achieve testing consistency under this scaling of n , the kernel bandwidth γ scales with $n^{-1/(d+2\beta)}$, which provides a theoretical answer to Question 2. The result holds for distributions p and q in the Hölder class $\mathcal{H}^\beta(\mathcal{M})$, $0 < \beta \leq 2$. We characterize the finite-sample level and the power of the kernel two-sample test, and show that the properties are only affected by the intrinsic dimensionality d rather than the ambient dimensionality m . This result indicates that kernel tests can avoid the curse-of-dimensionality for manifold data, echoing a similar result of KDE in [40]. When the kernel is positive semi-definite (PSD), the kernel test we study equals the RKHS kernel MMD statistic [21]. However, our analysis covers non-PSD kernel, where the only requirement of the kernel function is a regularity, decay and positivity condition, c.f. Assumption 3.3. We experimentally demonstrate the testing power with non-PSD kernels in Section 5.3.

We first prove the kernel test consistency result when data densities lie on a smooth manifold without boundary and then extended to submanifolds with a smooth boundary for Hölder class densities with $0 < \beta \leq 1$. (When $\beta > 1$, there is no more improvement in the rate due to the degenerate kernel integral at the manifold boundary.) The manifold with boundary setting contains, as a special case, when p and q are supported on a compact domain in \mathbb{R}^m (with smooth boundary), and then $d = m$. The theory also

Table 1: List of default notations

m	dimensionality of ambient space	L_ρ	Upper bound of Hölder constants of p and q on \mathcal{M}
d	intrinsic dimensionality of the manifold	ρ_{\max}	Uniform upper bound of p and q on \mathcal{M}
\mathcal{M}	d -dimensional manifold in \mathbb{R}^m	γ	kernel bandwidth parameter
dV	volume form on \mathcal{M}	K_γ	kernel applied to data, $K_\gamma(x, y) = h\left(\frac{\ x-y\ ^2}{\gamma^2}\right)$
$d_{\mathcal{M}}(x, y)$	manifold geodesic distance	h	a C^1 and decay kernel function on $[0, \infty)$, $h \geq 0$
$\ x - y\ $	Euclidean distance in \mathbb{R}^m	m_0	$m_0[h] := \int_{\mathbb{R}^d} h(u ^2) du$
p, q	data sampling densities on \mathcal{M}	Asymptotic Notations	
n_X, n_Y	number of samples in two-sample datasets X and Y respectively	$O(\cdot)$	$f = O(g)$: there exists $C > 0$ such that when $ g $ is sufficiently small, $ f \leq C g $.
n	$n = n_X + n_Y$	$O_x(\cdot)$	declaring the constant dependence on x .
ρ_X	$n_X/n \rightarrow \rho_X$		
β	Hölder class $\mathcal{H}^\beta(\mathcal{M})$		

extends when the manifold data are corrupted by an additive Gaussian noise in the ambient space \mathbb{R}^m . We theoretically show that as long as the coordinate-wise Gaussian noise level σ is less than γ/\sqrt{m} up to an absolute constant (γ being the kernel bandwidth parameter), the kernel tests computed from noisy data have the same theoretical consistency rate as from the clean data which lie on the manifold. In this case, the test consistency is only determined by the pair of two densities of the clean manifold data.

Experimentally, we show that the test power can be maintained (for fixed test level) as the ambient dimensionality m increases for low-dimensional manifold data embedded in the high-dimensional space. The example that we construct consists of group transformed images with increasingly refined resolution (that is, increasing image size). We also conduct experiments on noise corrupted data, where, in the theoretical regime of small additive noise, the performance of kernel test on noisy data are similar to that on the clean data, as predicted by the theory. Next, we apply kernel tests to the more complicated hand-written digits dataset (which no longer lie on any known manifolds) and show that kernel bandwidth much smaller than the median distance bandwidth can give better performance. Finally, we investigate non-PSD kernels, which may or may not satisfy the proposed theoretical conditions.

2 Notation and preliminary

Following the setup in (1), we define $n := n_X + n_Y$, and our analysis considers finite n which is sufficient large. We also assume that n_X and n_Y are proportional, that is, as n increases, n_X/n approaches $\rho_X \in (0, 1)$.

2.1 Classical RKHS Kernel MMD statistic

The (biased) empirical estimate for the squared kernel MMD statistic [21] is defined as

$$\hat{T} := \frac{1}{n_X^2} \sum_{i, i'=1} K_\gamma(x_i, x_{i'}) + \frac{1}{n_Y^2} \sum_{j, j'=1} K_\gamma(y_j, y_{j'}) - \frac{2}{n_X n_Y} \sum_{i, j} K_\gamma(x_i, y_j), \quad (2)$$

where $K_\gamma(x, y)$ is a PSD kernel with a user-specified *bandwidth* parameter $\gamma > 0$. In this work, we consider a kernel with a fixed bandwidth, that is,

$$K_\gamma(x, y) = h\left(\frac{\|x - y\|^2}{\gamma^2}\right), \quad h : [0, \infty) \rightarrow \mathbb{R}, \quad (3)$$

where h usually is some non-negative function. A prototypical case is the Gaussian Radial Basis Function (RBF) kernel with $h(r) = \exp(-r/2)$. Classical theory of kernel MMD test requires the kernel to be

characteristic so that the MMD distance is a metric of distributions [21]. In this work, we use the test statistic (2), but only assume that h is a non-negative, C^1 and decaying function, which may not lead to a PSD kernel K_γ , see Assumption 3.3 and the comments in below.

The unbiased estimator of the kernel MMD removes the diagonal entries $K(x_i, x_i)$ and $K(y_j, y_j)$ in the summation in (2), and has a slightly different normalization (by $1/(N(N-1))$) rather than $1/N^2$, where $N = n_X$ and n_Y respectively). Since diagonal entries always equal $h(0)$, which is a constant, the biased and unbiased estimators give qualitatively the same behavior in our setting. In this paper, we focus on the biased estimator (2), and the analysis can be extend to the unbiased estimator.

2.2 Test level and power

Our concepts of the test level α_{level} and the testing power follow the standard statistical definitions [21]. For the two-sample test setting, one computes the kernel test statistic \hat{T} from datasets X and Y , and choose a threshold t_{thres} . The test rejects the null H_0 when $\hat{T} > t_{\text{thres}}$.

We denote the ‘‘level’’ of a test as α_{level} , which is also the target Type-I error. A test achieves a level α_{level} if

$$\mathbb{P}[\hat{T} > t_{\text{thres}} | H_0] \leq \alpha_{\text{level}}, \quad (4)$$

and here, $0 < \alpha_{\text{level}} < 1$ is typically set to a small constant; e.g., $\alpha_{\text{level}} = 0.05$. To control the Type-I error (4), the threshold t_{thres} needs to be greater than the $(1 - \alpha)$ -quantile of the distribution of \hat{T} under H_0 . In theory, t_{thres} can be determined by the limiting distribution of the detection statistic \hat{T} under H_0 , which is typically χ^2 in many scenarios. In practice, it is usually estimated by a standard boot-strap procedure [21, 27].

The Type-II error of the statistic \hat{T} and the threshold t_{thres} is given by $\mathbb{P}[\hat{T} \leq t_{\text{thres}} | H_1]$. The *testing power* (at level α_{level}) corresponds to one minus Type-II error. Given \hat{T} and t_{thres} such that (4) holds, the testing power (with respect to alternative q) is defined as

$$\pi(p, q; \hat{T}, t_{\text{thres}}) = \mathbb{P}[\hat{T} > t_{\text{thres}} | H_1 \text{ with } q]. \quad (5)$$

We call the test *asymptotically consistent*, of the testing power π can approach 1 as samples n increases. In the following, we will characterize the testing power of kernel test for a finite sample size n .

2.3 Other notations

A list of default notations is summarized in Table 1, and the notations are also declared in the text. We clarify the big-O notation used in the paper: Our main result holds for large enough sample size n and small enough kernel bandwidth γ and does not require $n \rightarrow \infty$. For convenience, we use big-O notations in in some lemmas and proof. Specifically, $f = O(|g|)$ means that there is constant C such that when $|g|$ is smaller than a threshold (g not necessarily converge to zero), $|f| \leq C|g|$. We may declare the needed smallness threshold of $|g|$, and when the condition is satisfied, the $O(|g|)$ term has absolute value bounded by $C|g|$. We subscript ‘‘x’’ in $O_x(\cdot)$ to denote that the constant C in big-O depends on object x . In this work, we treat constants which depend on manifold \mathcal{M} and kernel function h as absolute ones, and mainly track the constant dependence on data densities p and q . We clarify constant dependence in the text.

3 Kernel two-sample statistics for manifold data

In this section, we first set up the problem for kernel two-sample test for manifold data, introduce the local kernel, and present the main result about the test size and power.

3.1 Manifold data in high-dimensional space

We introduce needed assumptions on the manifold data and sampling densities. We start from compact manifold without boundary for simplicity:

Assumption 3.1 (Manifold assumption). *\mathcal{M} is a d -dimensional compact C^∞ manifold isometrically embedded in \mathbb{R}^m without boundary.*

The theory extends when manifold has smooth boundary by adopting similar analysis techniques, which will be discussed in Section 4.1. Let $\iota : \mathcal{M} \rightarrow \mathbb{R}^m$ be the isometric embedding, which is a C^∞ mapping. We use the same notation x to stand for a point $x \in \mathcal{M}$ and $\iota(x) \in \mathbb{R}^m$ when there is no danger of confusion. The ambient space \mathbb{R}^m has a dimensionality m possibly much larger than the intrinsic manifold dimensionality d . We denote by $d_{\mathcal{M}}(x, y)$ the geodesic distance on \mathcal{M} , and use $\|x - y\|$ for the Euclidean distance in \mathbb{R}^m . Let dV be the volume form on \mathcal{M} : when \mathcal{M} is orientable, dV is the Riemann volume form; otherwise, dV is the measure associated with the local volume form. In both cases, we have (\mathcal{M}, dV) as a measure space.

In this section, we assume that data densities p and q are supported on \mathcal{M} . Extension to when data lie near to the manifold will be discussed in Section 4.2, where our analysis covers the case of additive Gaussian noise as long as the noise level is below certain threshold determined by the kernel bandwidth. Start from the case where the densities p and q are on the manifold, we assume that they are in the Hölder class $\mathcal{H}^\beta(\mathcal{M})$, $0 < \beta \leq 2$, which means that

(i) When $\beta \leq 1$,

$$\mathcal{H}^\beta(\mathcal{M}) = \{f \in C^0(\mathcal{M}), \exists L > 0, |f(x) - f(y)| \leq L d_{\mathcal{M}}(x, y)^\beta, \forall x, y \in \mathcal{M}\}, \quad (6)$$

and we define the Hölder constant of f as $L_f := \sup_{x, y \in \mathcal{M}} |f(x) - f(y)| / d_{\mathcal{M}}(x, y)^\beta$.

(ii) When $1 < \beta \leq 2$,

$$\begin{aligned} \mathcal{H}^\beta(\mathcal{M}) = \\ \{f \in C^1(\mathcal{M}), \exists L > 0, \|\nabla_{\mathcal{M}} f(x) - \nabla_{\mathcal{M}} f(y)\| \leq L d_{\mathcal{M}}(x, y)^{\beta-1}, \forall x, y \in \mathcal{M}\}, \end{aligned} \quad (7)$$

and the we define $L_f := \|\nabla_{\mathcal{M}} f\|_\infty + \sup_{x, y \in \mathcal{M}} \|\nabla_{\mathcal{M}} f(x) - \nabla_{\mathcal{M}} f(y)\| / d_{\mathcal{M}}(x, y)^{\beta-1}$.

Our notion of the Hölder constant L_f removes the C^0 norm $\|f\|_\infty$ from the usual definition of the Hölder norm. When $\beta = 1$, L_f is the Lipschitz constant of f (with respect to manifold distance).

Assumption 3.2 (Data density assumption). *Data densities p and q are in $\mathcal{H}^\beta(\mathcal{M})$, $0 < \beta \leq 2$, and the Hölder constants of p and q are bounded by L_ρ . Since Hölder continuity implies continuity, due to compactness of \mathcal{M} , both densities are uniformly bounded, that is, there is constant ρ_{\max} such that*

$$0 \leq p(x), q(x) \leq \rho_{\max}, \quad \forall x \in \mathcal{M}.$$

To illustrate that the manifold structure naturally arises in real data, we give an example of high-dimensional data which lie on intrinsically low-dimensional manifolds. In addition, in this example the change of data densities q from p are induced by the change of densities on a latent manifold independent of the ambient space \mathbb{R}^m .

Example 1 (Manifold data with increasing m). Let data samples be images I_i which have $W \times W$ pixels, and thus vectors in \mathbb{R}^m , $m = W^2$. The image I_i is produced by evaluating a continuous function on an image grid, that is,

$$I_i(j_1, j_2) = F \left(\left(\frac{j_1}{W}, \frac{j_2}{W} \right); z_i \right), \quad 1 \leq j_1, j_2 \leq W,$$

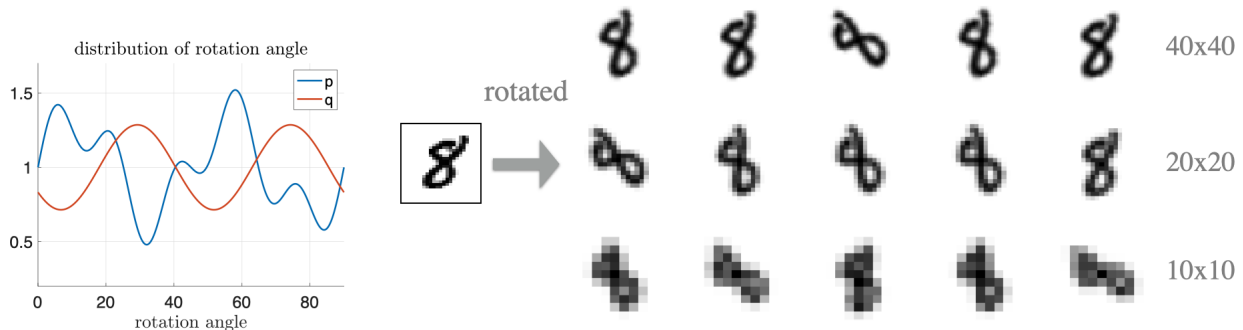


Figure 1: A constructed example to demonstrate that the increase in the ambient dimension m does not affect the intrinsic dimensionality d nor the intrinsic geometry of the manifold data. An image of hand-written digit “8” is rotated by angles z from 0 to 90 degrees, and at different image sizes. The images for $z \in [0, \pi/2]$ lie on a one-dimensional manifold in the ambient space, and approaches a certain continuous limit as image resolution refines. The group element z have two distributions, which induce two distributions of data images in ambient space \mathbb{R}^m . The two-sample test results on this data are provided in Section 5.

where $F(u; z_i)$ is a smooth mapping from $u \in [0, 1] \times [0, 1]$ to \mathbb{R} and is parametrized by a latent variable $z_i \in \mathcal{M}_z$. For example, let \mathcal{M}_z be a rotation group $SO(2)$, and the mapping $F(\cdot; z)$ corresponds to applying rotation action $z \in SO(2)$ to the image, as illustrated in Figure 1. Suppose \mathcal{M}_z is d -dimensional, then, under generic assumptions on F , the continuous functions $F(\cdot; z)$ for all z lies on a d -dimensional manifold in the function space, and when the discretization is fine enough, the images I_i lie on a manifold in $\mathbb{R}^{W \times W}$ which approaches the manifold of continuous functions in the limit of $W \rightarrow \infty$. When the two distributions p and q of images I_i on the image manifold are induced by densities p_z and q_z which are distributions of z_i on \mathcal{M}_z , the latter does not change with W . Consequently, as dimensionality m increases, the Kullback-Leibler divergence $\text{KL}(p||q)$ approaches $\text{KL}(p_z||q_z)$ which is an $O(1)$ limit.

3.2 Local kernels on manifold

Same as in the setting of traditional manifold learning analysis [18, 4, 53], we consider local kernel $K_\gamma(x, y)$ defined as in (3), where typically the bandwidth parameter γ decreases as number of data samples n increases. In the term of “local kernel”, “local” means a small kernel bandwidth γ . The following class of non-negative differential kernel function h contains Gaussian RBF kernel as a special case.

Assumption 3.3 (Differentiable kernel). *We made the following assumptions about the function h , excluding the case where $h \equiv 0$:*

(C1) *Regularity.* h is continuous on $[0, \infty)$, C^1 on $(0, \infty)$.

(C2) *Decay condition.* h and h' are bounded on $(0, \infty)$ and have sub-exponential tail, specifically, $\exists a, a_k > 0$, s.t., $|h^{(k)}(\xi)| \leq a_k e^{-a\xi}$ for all $\xi > 0$, $k = 0, 1$. Without loss of generality, assume that $a_0 = 1$.

(C3) *Non-negativity.* $h \geq 0$ on $[0, \infty)$.

Similar conditions on h have been used in [18] for kernelized graph Laplacian constructed from manifold data. For h that satisfies Assumption 3.3, we introduce the following moment constant of the kernel h ,

$$m_0[h] := \int_{\mathbb{R}^d} h(\|u\|^2) du,$$

which is finite due to (C2). By (C1)(C3) and that h is not a zero function, $m_0[h] > 0$. Condition (C2) implies that $|K_\gamma(x, y)| \leq 1$ for any x, y , where $K_\gamma(x, y)$ is induced by h as defined in (3). Note that

the kernel $K_\gamma(x, y)$ is not necessarily PSD, a situation where the theory herein remain valid. (For the prototypical choice of the Gaussian RBF kernel, the kernel is indeed PSD.) The non-negativity condition (C3) may be relaxed, as it is only used to guarantee that $m_0[h] > 0$ and in the extension to manifold with boundary in Section 4.1. We assume (C3) for simplicity.

The following lemma establishes the approximation of the integral of Hölder function with local kernel on a manifold.

Lemma 3.1. *Suppose \mathcal{M} satisfies Assumption 3.1, h satisfies Assumption 3.3, and f is in $\mathcal{H}^\beta(\mathcal{M})$, $0 < \beta \leq 2$, with Hölder constant L_f . Then there is $\gamma_0 > 0$ which depends on \mathcal{M} only, and constant C_1 that depends on (\mathcal{M}, h) , such that when $0 < \gamma < \min\{1, \gamma_0\}$,*

$$\begin{aligned} & \left| \gamma^{-d} \int_{\mathcal{M}} h\left(\frac{\|x-y\|^2}{\gamma^2}\right) f(y) dV(y) - m_0[h]f(x) \right| \\ & \leq C_1(L_f \gamma^\beta + \|f\|_\infty \gamma^2), \quad \forall x \in \mathcal{M}. \end{aligned} \quad (8)$$

Specifically, γ_0 depends on manifold reach and curvature, and $C_1 > 0$ depends on manifold curvature and volume, the kernel function h (including the constants a, a_1 in Assumption 3.3(C2)), and the intrinsic dimensionality d .

When $L_f > 0$, since $\beta \leq 2$, the $O(\gamma^\beta)$ term will be the leading term in the r.h.s of (8). When $\beta = 2$, the residual term in (8) becomes $O(\gamma^2)$, which echos the $O(\gamma^2)$ error term in Lemma 8 of [18], and the latter was proved for f with higher order regularity and under different technical assumptions. The proof follows the approach in [18] using standard technique of differential geometry, and is included in Section 7 for completeness.

The empirical test statistic \widehat{T} is as in (2). We also define the population kernel test statistic

$$\begin{aligned} T & := \mathbb{E}_{x \sim p, y \sim p} K_\gamma(x, y) + \mathbb{E}_{x \sim q, y \sim q} K_\gamma(x, y) - 2\mathbb{E}_{x \sim p, y \sim q} K_\gamma(x, y) \\ & = \int_{\mathcal{M}} \int_{\mathcal{M}} K_\gamma(x, y) (p - q)(x)(p - q)(y) dV(x) dV(y), \end{aligned} \quad (9)$$

which equals the population (squared) kernel MMD when K_γ is PSD. We apply Lemma 3.1 to when $f = p$ or q to obtain the following lemma, which is proved in Section 7.

Lemma 3.2. *Under Assumption 3.1, 3.2, 3.3, γ_0 and C_1 as in Lemma 3.1, then when $0 < \gamma < \min\{1, \gamma_0\}$,*

$$T = \gamma^d \left(m_0[h] \int_{\mathcal{M}} (p(x) - q(x))^2 dV(x) + r_T \right), \quad |r_T| \leq 4C_1(L_\rho \gamma^\beta + \rho_{\max} \gamma^2). \quad (10)$$

3.3 Control of deviation of \widehat{T} from mean

We now control the deviation \widehat{T} around certain expected value (with bias) using concentration of U-statistics. As our analysis considers sufficiently large samples, without loss of generality, we assume that the following *balance-ness condition* holds for all n ,

$$0.9\rho_X \leq \frac{n_X - 1}{n}, \quad 0.9(1 - \rho_X) \leq \frac{n_Y - 1}{n}, \quad 0 < \rho_X < 1. \quad (11)$$

The U-statistic argument was used in [21] but only using the point-wise boundedness of the kernel. To obtain better concentration, we apply the Bernstein-type argument which allows to reveal the role of the bandwidth. The proof adopts the classical decoupling technique of the U-statistics [28], and is included in Section 7 for completeness.

Proposition 3.4. *Under Assumption 3.1, 3.2, 3.3, and the balance-ness condition (11). Define*

$$c := 0.9 \min\{\rho_X, 1 - \rho_X\}, \quad \nu := (m_0[h^2] + 1)\rho_{\max}. \quad (12)$$

Then, there is a constant $C_1^{(2)} > 0$ which depends (\mathcal{M}, h) , such that when $0 < \gamma < \min\{1, \gamma_0, (C_1^{(2)})^{-1/2}\}$,

(1) Under H_0 , for $0 < \lambda < 3\sqrt{c\nu\gamma^d n}$, w.p. $\geq 1 - 3e^{-\lambda^2/8}$,

$$\widehat{T} \leq \frac{4}{cn} + 4\lambda\sqrt{\frac{\nu\gamma^d}{c n}},$$

(2) Under H_1 , let T be defined as in (9), for $0 < \lambda < 3\sqrt{c\nu\gamma^d n}$, w.p. $\geq 1 - 3e^{-\lambda^2/8}$,

$$\widehat{T} \geq T - 4\lambda\sqrt{\frac{\nu\gamma^d}{c n}}.$$

The constant $C_1^{(2)}$ corresponds to the constant C_1 in Lemma 3.1 with the kernel function h replaced by h^2 .

The proof of Proposition 3.4 is left to Section 7. Because that analysis uses U-statistic argument, it obtains $O(n^{-1/2})$ fluctuation of the statistics \widehat{T} around the mean (up to the $O(n^{-1})$ bias) under both H_0 and H_1 . Note that, under H_0 , the deviation can be expected to scale as $O(n^{-1})$ [21, 14]. While this could make a difference in terms of choosing test threshold t (if one uses the limiting density), it does not affect our proof of the testing power in Theorem 3.5, because the deviation of \widehat{T} under H_1 is of order $O(n^{-1/2})$ will be the dominating term over the deviation of \widehat{T} under H_0 . In practice, the testing threshold is usually estimated empirically by bootstrap methods rather than chosen according to theory, see more in Section 5. We thus postpone the improvement of the concentration of \widehat{T} under H_0 to current work.

3.4 Kernel test level and power

We are ready to derive the main theorem on kernel test's level and power at finite sample size:

Theorem 3.5 (Level and power of kernel test on manifold). *Under Assumptions 3.1, 3.2, 3.3, and the balance-ness condition (11), let the constants c , ν , and $C_1^{(2)}$ be as in Proposition 3.4, and γ_0 and C_1 as in Lemma 3.1. Define*

$$\lambda_1 = \sqrt{8 \log(3/\alpha_{\text{level}})},$$

and let the threshold for the test be

$$t_{\text{thres}} = \frac{4}{cn} + 4\lambda_1\sqrt{\frac{\nu}{c} \cdot \frac{\gamma^d}{n}}.$$

For $q \neq p$ under H_1 , define

$$D_{p,q} := m_0[h] \int_{\mathcal{M}} (p(x) - q(x))^2 dV(x) > 0.$$

Then, when γ is small enough such that

$$0 < \gamma < \min\left\{1, \gamma_0, (C_1^{(2)})^{-1/2}\right\}, \quad L_\rho\gamma^\beta + \rho_{\max}\gamma^2 < \frac{0.1D_{p,q}}{4C_1}, \quad (13)$$

and meanwhile, for some constant $\lambda_2 > 0$, n is large enough such that

$$\gamma^d n > \max\left\{\frac{1}{c\nu} \left(\frac{\max\{\lambda_1, \lambda_2\}}{3}\right)^2, \frac{10}{cD_{p,q}}, \frac{\nu}{c} \left(\frac{8(\lambda_1 + \lambda_2)}{D_{p,q}}\right)^2\right\}, \quad (14)$$

then

$$\mathbb{P}[\widehat{T} > t_{\text{thres}} | H_0] \leq \alpha_{\text{level}}, \quad \mathbb{P}[\widehat{T} \leq t_{\text{thres}} | H_1] \leq 3e^{-\lambda_2^2/8}. \quad (15)$$

Since the constants $m_0[h^2]$ appears in ν , and $m_0[h]$ appears in $D_{p,q}$, here we derive explicit constants for Gaussian RBF kernel.

Example 2 (Constants for Gaussian h). When $h(r) = e^{-r/2}$,

$$m_0[h] = \int_{\mathbb{R}^d} e^{-|u|^2/2} du = (2\pi)^{d/2}, \quad m_0[h^2] = \int_{\mathbb{R}^d} e^{-|u|^2} du = \pi^{d/2},$$

both of which are constants depending on d .

Theorem 3.5 considers a fixed alternative q , yet the bound of testing power holds for finite samples and finite γ , and thus the result can address certain asymptotic scenarios where $q - p$ decreases to zero as n increases. In Theorem 3.5, only the intrinsic dimensionality d affects the testing power but not the ambient space dimensionality m . The constants $D_{p,q}$, ρ_{\max} , and L_ρ are determined by p and q as Hölder functions on (\mathcal{M}, dV) , which are intrinsically defined.

Remark 3.1 (Condition for test consistency). Under the setting of manifold densities p and q , define

$$\delta_2 := \delta_2(p, q) = \int_{\mathcal{M}} (p(x) - q(x))^2 dV(x), \quad D_{p,q} = m_0[h] \delta_2.$$

We consider where δ_2 is small such that the third term in (14) achieves the maximum among the three, which requires $\delta_2 < c\nu$ for some $O(1)$ constant c . Here we treat λ_1 and λ_2 as $O(1)$ fixed constants. Theorem 3.5 implies that the kernel two-sample test is consistent and the test power approaches 1 exponentially fast as number of samples n increases if

- (i) γ can be chosen to be smaller than some $O(1)$ threshold determined by (\mathcal{M}, h) , and also small enough such that, for $c_1 > 0$ which depends on (L_ρ, ρ_{\max}) and $m_0[h]$,

$$\gamma^\beta < c_1 \delta_2,$$

Here we use the $O(\gamma^\beta)$ term in the condition (13) because $\beta \leq 2$.

- (ii) n is sufficiently large to make

$$\gamma^d n > \frac{c_2}{\delta_2^2},$$

where $c_2 > 0$ depends on ρ_{\max} , ρ_X and (\mathcal{M}, h) .

Putting together, it means that, for such small δ_2 , the threshold for n to give testing power is when

$$n \gtrsim \delta_2^{-2-d/\beta}, \quad \text{with } \gamma \sim n^{-1/(d+2\beta)} \tag{16}$$

up to constants which are omitted. This means that the smallest $\delta_2(p, q)$ that can be detected by the kernel test is $\delta_2 \gtrsim n^{-1/(2+d/\beta)}$. In particular, when $\beta = 2$, this becomes $\delta_2 \gtrsim n^{-1/(2+d/2)}$, and the choice of bandwidth γ is at the order of $n^{-1/(d+4)}$.

Remark 3.2 (Choice of bandwidth). As shown in (16), at the critical regime of detectability by the test where δ_2 is small, the bandwidth needs to scale with $n^{-1/(d+2\beta)}$ so that the test can have power. The scaling echos the classical theory of density estimation [54]. This choice of γ leads to local kernels for the manifold kernel test, where $\gamma \rightarrow 0$ as n increases. In contrast, the median distance choice of bandwidth [21] may lead to γ which is of $O(1)$: on a manifold of diameter $O(1)$, suppose the data density is uniform, then the median of pairwise distance is generally $O(1)$. Thus the median distance γ may not be optimal in practice for high-dimensional data, e.g., when data lie on or near to intrinsically low-dimensional manifold or sub-manifolds and there are sufficiently many samples in the dataset to detect a small departure of the density. We show in Section 5 that kernel tests with a smaller bandwidth may outperform that with the median distance bandwidth in experiments.

4 Theoretical extensions

4.1 Manifold with boundary

In this section, we show that the theoretical results in Section 3 extend when the data manifold \mathcal{M} has smooth boundary $\partial\mathcal{M}$, that is,

Assumption 4.1. \mathcal{M} is a d -dimensional compact C^∞ sub-manifold isometrically embedded in \mathbb{R}^m , where the boundary $\partial\mathcal{M}$ is also C^∞ .

The proof uses similar techniques, and is based on the local kernel integral lemma, Lemma 4.1, which handles when x is on or near to $\partial\mathcal{M}$. Theorem 3.5 then extends to data densities in Hölder class $\mathcal{H}^\beta(\mathcal{M})$ with $0 < \beta \leq 1$ with certain changes in the constants and condition (13) due to the degenerate approximation error terms at the manifold boundary in Lemma 4.1. See the specifics in below.

Remark 4.1. When data densities p and q are compactly supported on some domain Ω in \mathbb{R}^m and Ω has smooth boundary, this is a special case of the manifold-with-boundary setting where $d = m$. Our theoretical result thus covers such cases. When m is large, there is a curse-of-dimensionality revealed by the γ^d factor in the required lower bound of n in the condition (14).

We start by establishing the following lemma, which is the counter-part of Lemma 3.1 for $0 < \beta \leq 1$. All proofs in this subsection are left to Appendix 7.2.

Lemma 4.1. Suppose \mathcal{M} satisfies Assumption 4.1, h satisfies Assumption 3.3, and f is in $\mathcal{H}^\beta(\mathcal{M})$, $0 < \beta \leq 1$, with Hölder constant L_f . Let $d_E(x, \partial\mathcal{M})$ denote the Euclidean distance from $x \in \mathcal{M}$ to $\partial\mathcal{M}$, and define $\delta_\gamma := \sqrt{\frac{d+10}{a}\gamma^2 \log \frac{1}{\gamma}}$. Then, there is $\gamma'_0 > 0$ which depends on \mathcal{M} only, and constant C'_1 that depends on (\mathcal{M}, h) such that when $0 < \gamma < \min\{\gamma'_0, 1\}$, for any x such that $d_E(x, \partial\mathcal{M}) \leq \delta_\gamma$,

$$\begin{aligned} & \left| \gamma^{-d} \int_{\mathcal{M}} h \left(\frac{\|x-y\|^2}{\gamma^2} \right) f(y) dV(y) - m_0^{(\gamma)}[h](x) f(x) \right| \\ & \leq C'_1 (L_f \gamma^\beta + \|f\|_\infty \gamma^2), \end{aligned} \quad (17)$$

where $0 \leq m_0^{(\gamma)}[h](x) \leq m_0[h]$ for all x ; For any x such that $d_E(x, \partial\mathcal{M}) > \delta_\gamma$, (17) holds with $m_0^{(\gamma)}[h](x)$ replaced with $m_0[h]$.

Remark 4.2. Similarly as in Lemma 3.1, γ'_0 depends on manifold reach and curvature, and the constant C'_1 depends on manifold curvature and volume, and the kernel function h . When $1 < \beta \leq 2$, previously in Lemma 3.1 the $O(\gamma^\beta)$ term can further improve, however, when x is near or on the boundary $\partial\mathcal{M}$, even when f is C^1 , there will be a $O(\|\nabla_{\mathcal{M}} f\|_\infty \gamma)$ residual term due to that the integral of $h(\|u\|^2/\gamma^2)u$ on half of \mathbb{R}^d no longer vanishes. Thus we only derive the bound for $\beta \leq 1$ here.

We then extend Lemma 3.2 which bounds the error between $\gamma^{-d}T$ and $m_0[h]C_{p,q}$:

Lemma 4.2. Under Assumptions 4.1, 3.3, densities p and q as in Assumption 3.2 with $0 < \beta \leq 1$, γ'_0 and C'_1 as in Lemma 4.1. Then, when $0 < \gamma < \min\{1, \gamma'_0\}$, we have that

$$\begin{aligned} T &= \gamma^d \left(m_0[h] \int_{\mathcal{M}} (p(x) - q(x))^2 dV(x) + r_T \right), \\ |r_T| &\leq 4 \left(C'_1 (L_\rho \gamma^\beta + \rho_{\max} \gamma^2) + C'_2 \rho_{\max}^2 \gamma \sqrt{\log \frac{1}{\gamma}} \right), \end{aligned} \quad (18)$$

where the constant C'_2 depends on manifold curvature, the regularity and volume of the manifold boundary $\partial\mathcal{M}$, the intrinsic dimensionality d and the kernel function h .

Finally, to extend Proposition 3.4, it suffices to bound the integral

$$\mathbb{E}_{x \sim p, y \sim p} K_\gamma(x, y)^2 \leq \nu \gamma^d, \quad (19)$$

where ν is defined as in (12). We prove in Appendix 7.2 that this is the case when $\gamma < (C_1^{\prime(2)})^{-1/2}$, where $C_1^{\prime(2)}$ corresponds to the constant C_1' in Lemma 4.1 replacing h with h^2 , and thus $C_1^{\prime(2)}$ only depends on (\mathcal{M}, h) . The upper bounds of $\mathbb{E}_{x \sim q, y \sim q} K_\gamma(x, y)^2$ and $\mathbb{E}_{x \sim p, y \sim q} K_\gamma(x, y)^2$ are similar. Thus the same deviation bound as in Proposition 3.4 can be proved after replacing the constants $C_1^{(2)}$ with $C_1^{\prime(2)}$, and γ_0 with γ'_0 , in the statement. The main theorem Theorem 3.5 then directly follows, with the following changes: (i) replacements of the constants $\gamma_0, C_1, C_1^{(2)}$ with those with primes, (ii) Condition (13) is replaced by $4 \left(C_1' (L \rho \gamma^\beta + \rho_{\max} \gamma^2) + C_2' \rho_{\max}^2 \gamma \sqrt{\log \frac{1}{\gamma}} \right) < 0.1 D_{p,q}$, due to the extra error term involving C_2' in Lemma 4.2.

We have extended the theory to data manifold with smooth boundary. In line with the theoretical results, the experiments in Section 5 are conducted on manifold data where \mathcal{M} has boundary. In Section 5.1, the data manifold is a continuous curve in the ambient space with endpoints. In Section 5.2, the original MNIST image data lie close to a collection of sub-manifolds in the ambient space, and it is also a case of manifold with boundary.

4.2 Near-manifold data

In applications, data points may not lie exactly on the low-dimensional manifold but only near to it. Since kernel $K_\gamma(x, y)$ is computed from Euclidean distances among data points, one can expect that if data samples are lying within distance proportional to γ from the manifold \mathcal{M} , then the integration of kernel $K_\gamma(x, y)$ over such data distributions will preserve the magnitude to be of order γ^d and will not have curse of dimensionality.

An important case is when near-manifold data are produced by adding Gaussian noise, which are distributed as $\mathcal{N}(0, \sigma^2 I_m)$, to data points which are lying on manifold. In this case, to make the off-manifold perturbation to be of length up to a constant times of γ (with high probability), it allows σ to be up to $c\gamma/\sqrt{m}$ for some $c > 0$. Here, we show that Theorem 3.5 can be extended under this noise regime for Gaussian kernel h . The analysis may also extend to other types of kernel functions.

Specifically, let $x_i = x_i^{(c)} + \xi_i^{(1)}$, $x_i^{(c)} \sim p_{\mathcal{M}}$, $\xi_i^{(1)} \sim \mathcal{N}(0, \sigma_{(1)}^2 I_m)$, and $y_i = y_i^{(c)} + \xi_i^{(2)}$, $y_i^{(c)} \sim q_{\mathcal{M}}$, $\xi_i^{(2)} \sim \mathcal{N}(0, \sigma_{(2)}^2 I_m)$, where the manifold clean data $x_i^{(c)}$ and $y_i^{(c)}$ are independent from the ambient space Gaussian noise $\xi_i^{(1)}$ and $\xi_i^{(2)}$. When $p_{\mathcal{M}}$ and $q_{\mathcal{M}}$ satisfies Assumption 3.2 and h is Gaussian kernel, Theorem 3.5 extends when, for some $c > 0$,

$$\sigma_{(1)}^2 + \sigma_{(2)}^2 \leq \frac{c^2}{m} \gamma^2. \quad (20)$$

The argument is based on that the proof of Theorem 3.5 relies on the approximation of kernel integrals $\mathbb{E}_{x \sim p, y \sim p} K_\gamma(x, y)$ and the boundedness of $\mathbb{E}_{x \sim p, y \sim p} K_\gamma(x, y)^2$ at the order $O(\gamma^d)$, and similarly with $\mathbb{E}_{x \sim p, y \sim q}$, $\mathbb{E}_{x \sim q, y \sim q}$. Thus, when kernel h is Gaussian, and p (and q) equals $p_{\mathcal{M}}$ (and $q_{\mathcal{M}}$) convolved with a Gaussian with coordinate variance $\lesssim \gamma^2/m$ in \mathbb{R}^m , these integrals can be shown to be equivalent to those integrated over $p_{\mathcal{M}}$ and $q_{\mathcal{M}}$ with another Gaussian kernel having bandwidth $\tilde{\gamma}$, where $\tilde{\gamma}/\gamma$ is bounded between 1 and the absolute constant $\sqrt{1 + c^2/m}$. As a result, the integrals of $K_\gamma(x, y)$ and $K_\gamma(x, y)^2$ can be computed same as before in Lemma 3.2 and Proposition 3.4, leading to a result of Theorem 3.5 after replacing the roles of p and q with $p_{\mathcal{M}}$ and $q_{\mathcal{M}}$. Details are left to Section 7.3.

This suggests that when the coordinate-wise noise level σ in \mathbb{R}^m is bounded at the level of γ/\sqrt{m} , the behavior of the two-sample test with kernel $K_\gamma(x, y)$ applied to manifold plus noise data is essentially close to as if applied to the clean data on the manifold, and the testing power is determined by the on-manifold distributions $p_{\mathcal{M}}$ and $q_{\mathcal{M}}$. Experiments of data with additive Gaussian noise are given in Section 5, which

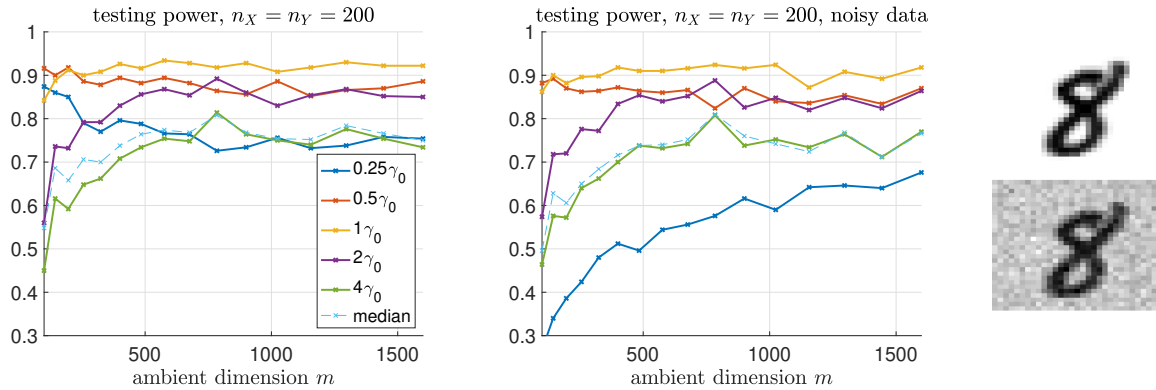


Figure 2: An example of simulated manifold data on which the kernel test power does not drop as the ambient dimension m increases, where the intrinsic dimension d remains constant. Gaussian kernel test statistics are computed on two datasets of rotated images with different distributions of rotation angles. Images are of sizes $10 \times 10, \dots, 40 \times 40$, and thus m increases from 100 to 1600. The test are computed with 5 values of kernel bandwidth as in (21), and that chosen by the median distance from data. The test power is estimated using $n_{\text{run}} = 500$. (Left) Results on clean images. (Middle) Results on images with additive Gaussian noise, where noise level is chosen to be small and satisfies the condition in Section 4.2. (Right) Example clean and noisy images (size 30×30).

verifies this theoretical prediction. In practice, with finitely many samples and dimensionality, the testing performances on clean and noisy data will stay close for small noise level σ , and start to have discrepancy when σ exceeds certain level allow by the theoretical range above.

5 Numerical experiments

In this section, we present several numerical examples to demonstrate the validity of our theory.¹ We first study a synthetic example of image data lying on a manifold, and then a density departure example using the MNIST dataset. The summary of the algorithm, including computation of the test threshold by bootstrap [1], is provided in Appendix A. The notations are as follows: n_{run} is the number of replicas used to estimate the test power, and n_{boot} the number of bootstrap samples in computing the test threshold. We set the test level $\alpha_{\text{level}} = 0.05$ throughout.

In our experiments, we test over a range of kernel bandwidth parameters γ . In practice, γ can also be chosen adaptively from data, e.g., the *median distance bandwidth* is set to be the median of all pairwise distances in the two sample datasets. Our theory in Section 3 suggests that the median distance γ may not always be the optimal choice: for manifold data of intrinsically low dimensionality, kernels with smaller bandwidth can achieve better testing power when there are sufficiently many samples. We verify this in experiments. In addition, we examine Gaussian kernel and several possibly non-PSD kernels, and verify that the latter can also achieve high test power as suggested by our theory.

5.1 Images with differently distributed rotation angles

5.1.1 Clean data

We construct two datasets consisting of randomly rotated copies of a digit image which are resized to be of different resolutions. The data generating process was introduced in Example 1 and illustrated in Figure 1. The distributions p and q of the two datasets are induced by different rotation angle distributions, and the densities of rotation angles (between 0 to 90 degrees) are shown in the left of Figure 1. The image sizes

¹Code available at the public repository https://github.com/xycheng/manifold_mmd.

change from 10×10 to 40×40 , and as a result, the data dimensionality increases from 100 to 1600. Note that since the rotation is only up to $\pi/2$, the corresponding manifold is a 1D curve with two endpoints, namely a manifold with boundary.

Note that the image pixels values maintain the same magnitude as W increases, and then the value of $\frac{1}{m} \sum_{u=1}^m I_i(u)^2$ approaches an $O(1)$ limit, which is the squared integral of the underlying continuous function on $[0, 1]^2$. This means that the image data vectors of size $W \times W$ need to divide by \sqrt{m} , $m = W^2$, so as to obtain isometric embedding of a manifold of diameter $O(1)$ in \mathbb{R}^m . In experiments we use bandwidth γ to resized images, can we call γ/\sqrt{m} the “pixel-wise bandwidth”. The pixel-wise bandwidth corresponds to the “ γ ” in the theory in Section 3.

In computing the Gaussian kernel test statistics, we use bandwidth parameter over 5 values such that

$$\frac{\gamma}{\sqrt{m}} = \gamma_0 \left\{ \frac{1}{4}, \frac{1}{2}, 1, 2, 4 \right\}, \quad m = W^2, \quad W = 10, \dots, 40, \quad (21)$$

with $\gamma_0 = 20$, which we call the “baseline pixel-wise bandwidth”. The median distance gives the pixel-wise bandwidth about 70. Since the grayscale images take pixel values between 0 and 255, the pixel-wise bandwidth being 20 is relatively small, and is smaller than that chosen by the median distance. The estimated two-sample testing power on clean images is shown in Figure 2 (Left), which is computed using $n_{\text{boot}} = 400$ and $n_{\text{run}} = 500$. It can be seen that all the bandwidth choices give certain test power, which is consistent across m as m increases (showing a tendency of convergence after m exceeds 500 till 1600). The performance with pixel-wise bandwidth equals 20 appears to be the best and is better than the bandwidth by median distance.

5.1.2 Noisy data

We add pixel-wise Gaussian noise of standard deviation $\sigma_0 = 20$ to the resized image data of dimension m , that is, $\sigma_0 = \gamma_0$ the baseline pixel-wise bandwidth in the previous clean data experiment. This falls under the scenario in Section 4.2: As was pointed in the experiment with clean data, normalized clean image I_i/\sqrt{m} lie on an $O(1)$ manifold, where I_i has size $W \times W$, $m = W^2$, and thus the pixel-wise bandwidth corresponds to the “ γ ” in the theory, If we add Gaussian noise $\mathcal{N}(0, \sigma_0^2 I_m)$ to the clean image I_i , it corresponds to adding noise $\mathcal{N}(0, (\sigma_0^2/m)I_m)$ to I_i/\sqrt{m} . Thus σ_0/\sqrt{m} is the “ σ ” in Section 4.2. The small noise regime in Section 4.2 requires “ $\sigma < c\gamma/\sqrt{m}$ ” for some constant c , and here, “ γ ” there is γ_0 , and “ σ ” there is σ_0/\sqrt{m} , thus the condition translates into $\sigma_0/\sqrt{m} < c\gamma_0/\sqrt{m}$, which is satisfied if we set $\sigma_0 = \gamma_0$.

An example pair of clean and noise-corrupted images are shown in Figure 2 (Right). We conduct the two-sample testing experiments in the same way as in the experiment with clean data, and the the estimated testing power is shown in Figure 2 (Middle). The performance with the four pixel-wise bandwidth which is greater than $\gamma_0/2$ are about the same as on the clean data; With the smallest pixel bandwidth $\gamma_0/4$, the test power degenerates and becomes worse than the choice by median distance, and the drop is more significant when dimensionality m is small. This suggests that this kernel bandwidth is too small for the amount of additive noise at the values of m and sample size n_X and n_Y .

5.2 Density departure in MNIST dataset

In this experiment, we compute Gaussian kernel two-sample test on the original MNIST digit image dataset, where samples are of dimensionality 28×28 . The data densities p and q are generated in the following way: p is uniformly subsample from the MNIST dataset, namely $p = p_{\text{data}}$. Though we only have finite samples (the MNIST dataset has 70000 images in 10 classes) of p_{data} , as we subsample $n_X = 6000$ from the whole dataset, it is approximate as if drawn from the population density. q is constructed as a mixture of $q = 0.975p_{\text{data}} + 0.025p_{\text{cohort}}$, where p_{cohort} is the distribution of a local cohort within the samples of digit “1”, having about 1700 samples. Since n_Y is set to be about 6000, and we subsample about

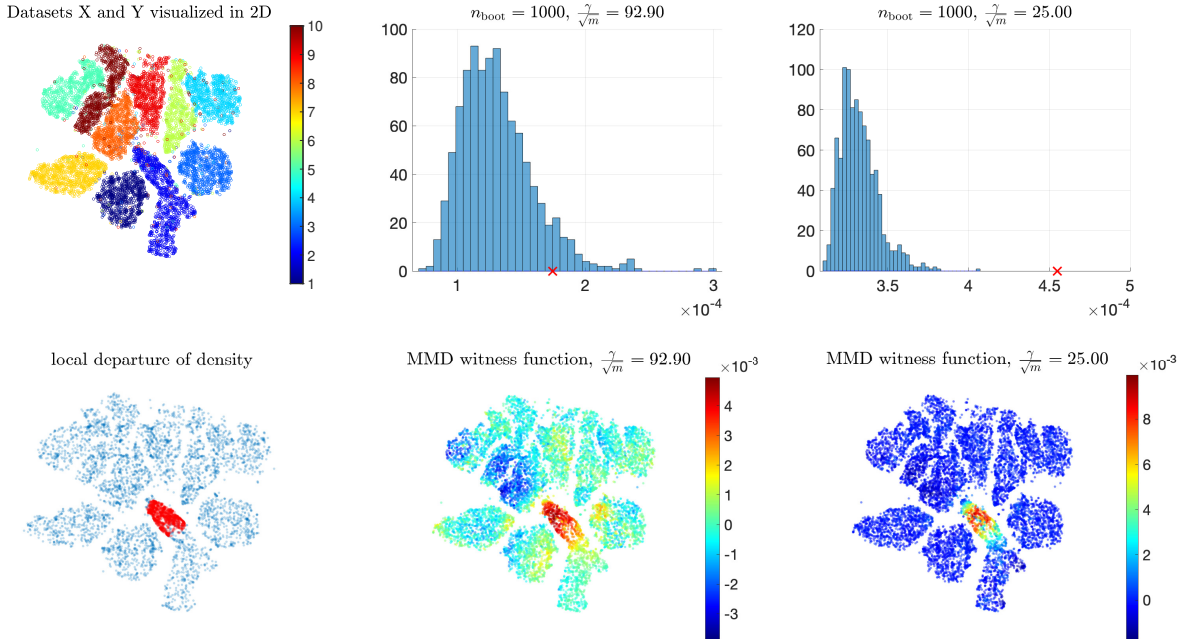


Figure 3: Kernel two-sample test to detect a local density departure of the MNIST image data distributions. (Top left) Dataset X and Y visualized in 2D by tSNE, colored by 10 digit class labels. (Top middle and right) Kernel test statistic \hat{T} (red cross) plotted against the histogram of test statistic under H_0 computed by bootstrap [1] (blue bar, see more in Appendix A). The middle plot is for Gaussian kernel test using median distance γ , and right plot is by using a smaller γ . (Bottom left) The local cohort density p_{cohort} illustrated by red dots. (Bottom middle and right) The witness function defined in (22) for kernel using median distance γ and a smaller bandwidth respectively.

150 from the local cohort, thus it is approximately drawn from the density of p_{cohort} . The local departure of density is illustrated in Figure 3 (Bottom left). The experiment are conducted on one realization of dataset X and Y , where $n_X = 6000$, $n_Y = 5990$.

We apply the kernel test with two bandwidths, one using the median distance, which gives the pixel-wise bandwidth $\gamma/\sqrt{m} = 92.9$, and here $m = 28^2$; and the other takes $\gamma/\sqrt{m} = 25$. The test statistic \hat{T} under H_1 vs. the histogram under H_0 computed by bootstrap with $n_{\text{boot}} = 1000$ are shown in the top panel of Figure 3. It can be seen that with the smaller bandwidth, the test statistic shows a more clear rejection of H_0 , indicating better testing power.

The *witness function* of kernel MMD [21] is defined as

$$\hat{w}(x) = -\frac{1}{n_X} \sum_{i=1}^{n_X} K_\gamma(x, x_i) + \frac{1}{n_Y} \sum_{j=1}^{n_Y} K_\gamma(x, y_j), \quad (22)$$

and we visualize \hat{w} with the Gaussian kernel as heat-map on the 2D embedding in the bottom panel of Figure 3. The witness function indicates where the two densities differ. Compared with the ground truth in the bottom left plot of the departure p_{cohort} , the witness function computed with the local kernel better detects the density departure than the median distance kernel, and this is consistent with the better test statistic separation in the top panel plots.

As a remark, unlike in Section 5.1, the MNIST image data do not lie on any constructed manifold induced by latent group action, but only lie near to certain manifold-like structures in the ambient space - the latent manifold reveals all possible variations of images of the 10 digits, and since there are 10 classes,

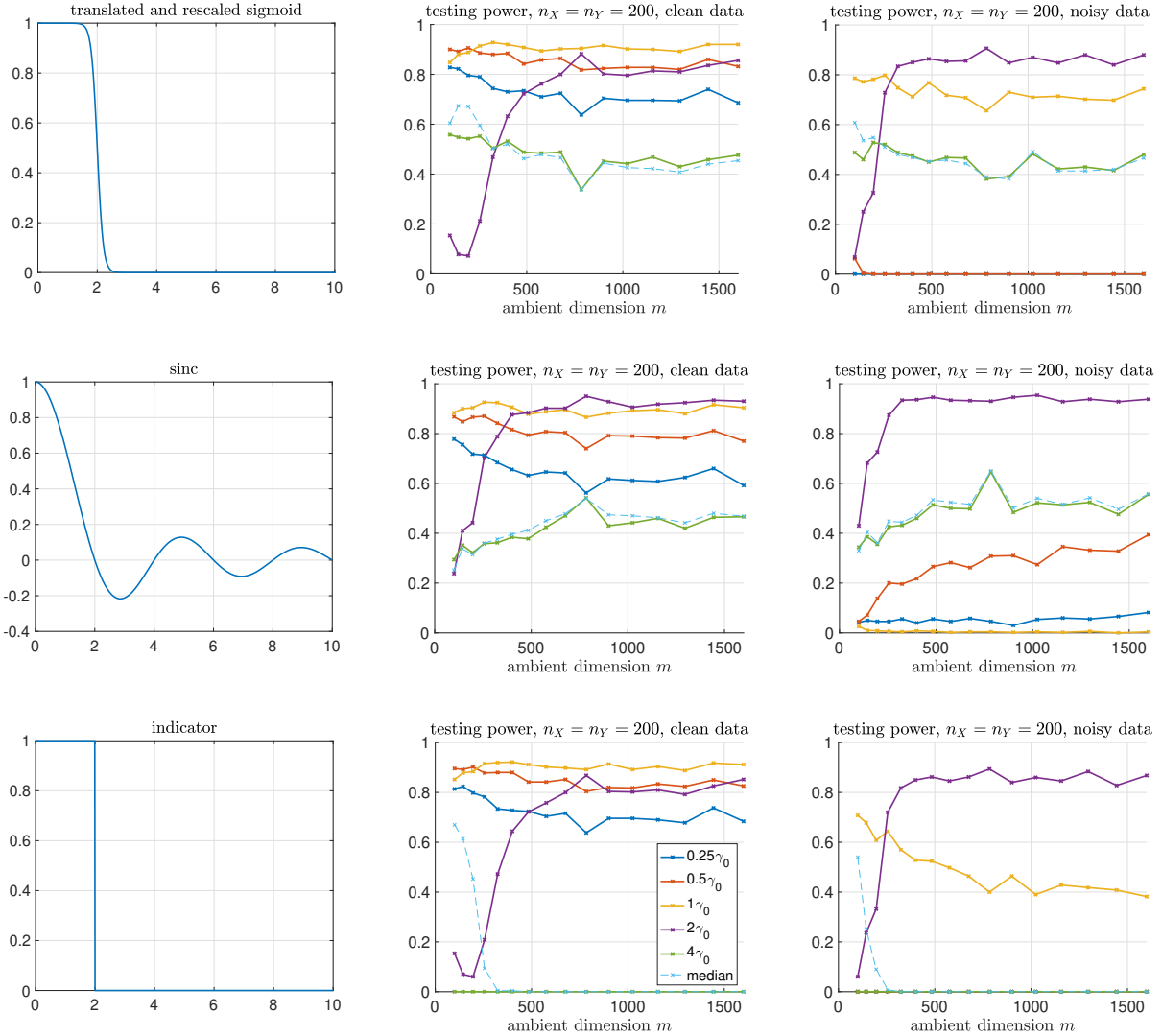


Figure 4: Two-sample test with non-Gaussian kernels that may not be PSD. (Left column) Three choices of kernel function h as in Section 5.3. (Right two columns) Same plots of testing powers on clean and noisy data of rotated images as in Figure 2, of the three kernel functions respectively.

there are possibly 10 sub-manifolds, as illustrated by the 2D embedding by tSNE [52] in Figure 3 (Top left). Thus, the case does not fall under the exact theoretical assumption of manifold data in Section 3, though manifold-like structures are likely to present in the dataset. The experimental results show that a more localized kernel that has a smaller bandwidth than the median distance bandwidth can have better testing power when applied to general manifold-like high-dimensional data.

5.3 Two-sample tests with non-PSD kernels

Using the same data and experimental set-up as in Section 5.1, we examine different choices of the kernel function h which are non-Gaussian and possibly non-PSD. Specifically, we study

- Sigmoid kernel: $h(r) = \frac{\exp\{-10(r-2)\}}{1+\exp\{-10(r-2)\}}$, which is a translated and rescaled sigmoid function and satisfies Assumption 3.3, but generally gives a non-PSD kernel $K_\gamma(x, y)$ for data in \mathbb{R}^m .
- Sinc kernel: $h(r) = \sin(\frac{\pi}{2}r)/(\frac{\pi}{2}r)$, which takes both positive and negative values on $(0, \infty)$, and only has $1/r$ decay, violating both (C2) and (C3).
- Indicator kernel: $h(r) = \mathbf{1}_{[0,2)}(r)$, which is not continuous on $(0, \infty)$, violating (C1).

Plots of the kernel function $h(r)$ as univariate functions are shown in the left column of Figure 4. The testing power for clean and noisy data over a range of kernel bandwidth, including the median distance bandwidth, are shown in the right two columns (same plots as in Figure 2). The results show that these kernel tests, when kernel is non-PSD and even violates the theoretical assumption, can obtain testing power if the kernel bandwidth is properly chosen. In addition, the optimal bandwidth may not be the median distance: the best performance achieved by the three kernels for clean data is obtained with γ_0 or $2\gamma_0$ in (21), which is smaller than the median distance as explained in Section 5.1. With noisy data, the testing powers worsen, but the power achieved by the best bandwidth is again comparable to that on the clean data for all three kernels; though the best bandwidth takes a different value from that under the clean data (which can be anticipated based on the analysis in Section 7.3). Comparing the (translated and rescaled) sigmoid kernel and the indicator kernel in Figure 4, it can be seen that the smoothness of the kernel function leads to better noise robustness; On this data, the Gaussian kernel shows better noise robustness than the non-PSD kernels, comparing Figure 2 with Figure 4.

In all experiments here, the testing power is maintained as the data ambient dimension m increases and shows a tendency of convergence. Apart from the no curse-of-dimensionality for manifold data, the results also support the theoretical suggestion that the consistency and power of kernel two-sample tests do not require kernel to be PSD (and then the test statistic is no longer an RKHS MMD).

6 Discussion

The work can be extended in several directions. First, the theoretical assumption on kernel functions may be further relaxed. In addition, we only consider isotropic kernel with fixed bandwidth, and it would be of interest to generalize to other types of kernel used in practice, such as anisotropic kernel using local Mahalanobis distance and other non-Euclidean metrics, kernel with adaptive bandwidth [57, 15], asymmetric kernel with a reference set [31, 14], and so on. Algorithm-wise, it would be desirable to develop efficient kernel testing methods to reduce storage and computational costs. Next, it is natural to extend to other kernel based testing problems, e.g., goodness-of-fit tests [16, 30, 48], and general hypothesis tests. The reduction of sampling complexity by the intrinsic low-dimensionality of manifold data may also be beneficial therein. At last, a more systematic study is to be developed for near-manifold data in high dimension - possibly going beyond the Riemannian manifold data assumption - to capture the intrinsic low dimensionality, or low complexity, in the data distributions for testing problems.

7 Proofs

7.1 Proofs in Section 3

Proof of Lemma 3.1. We denote by $B_r^l(x)$ the Euclidean ball in \mathbb{R}^l of radius $r > 0$ centered at x . When $l = m$, we omit the superscript l and use $B_r(x)$ to denote the Euclidean ball in the ambient space \mathbb{R}^m . In big-O notation, we use subscript $_{MC}$ to emphasize constant dependence on manifold curvature, $_{MV}$ for that on manifold volume, and $_{GM}$ for that on ‘‘Gaussian moments’’ namely the up to the 4-th moments of normal densities in \mathbb{R}^d .

First, we use the sub-exponential decay of h to truncate the integral of $dV(y)$ in (8) on $\mathcal{M} \cap B_{\delta_\gamma}(x)$ only with an $O(\|f\|_\infty \gamma^{10})$ residual, where $\delta_\gamma := \sqrt{\frac{d+10}{a} \gamma^2 \log \frac{1}{\gamma}}$. This is because when $\|y - x\| \geq \delta_\gamma$, by Assumption 3.3(C2), $h(\frac{\|x-y\|^2}{\gamma^2}) \leq e^{-a\delta_\gamma^2/\gamma^2} = \gamma^{d+10}$, and then

$$\begin{aligned} |\gamma^{-d} \int_{\mathcal{M} \setminus B_{\delta_\gamma}(x)} h\left(\frac{\|x-y\|^2}{\gamma^2}\right) f(y) dV(y)| &\leq \gamma^{-d} \int_{\mathcal{M} \setminus B_{\delta_\gamma}(x)} \gamma^{d+10} |f(y)| dV(y) \\ &\leq \|f\|_\infty \text{Vol}(\mathcal{M}) \gamma^{10} = O_{MV}(\|f\|_\infty \gamma^{10}), \quad \forall x \in \mathcal{M}. \end{aligned} \quad (23)$$

Next, we use local expansion of f and kernel function to compute the integral of $dV(y)$ on $B_{\delta_\gamma}(x)$.

By compactness of \mathcal{M} , there is $\gamma_1(\mathcal{M})$ such that when $\gamma < \gamma_1$ and then δ_γ is sufficiently small, $B_{\delta_\gamma}(x) \cap \mathcal{M}$ is isomorphic to a ball in \mathbb{R}^d . This $\gamma_1(\mathcal{M})$ depends on manifold reach. Then the local chart is well defined, and we use the local projected coordinate on the tangent plane: Let ϕ_x be the projection to $T_x(\mathcal{M})$, for each $y \in \mathcal{M} \cap B_{\delta_\gamma}(x)$, $u = \phi_x(y - x)$. By that locally the normal coordinate and the projected coordinate s matches up to the 3rd order (c.f. Lemma 6 and 7 in [18], also see Lemma A.1 in [15])

$$\begin{aligned} d_{\mathcal{M}}(x, y) &= \|u\|(1 + O_{MC}(\|u\|^2)), \quad \|y - x\| = \|u\|(1 + O_{MC}(\|u\|^2)), \\ \left| \det \left(\frac{dy}{du} \right) \right| &= 1 + O_{MC}(\|u\|^2), \end{aligned} \quad (24)$$

where the constants are uniform for all x , due to compactness of \mathcal{M} . Thus, there is another $\gamma_2(\mathcal{M})$ such that when $\gamma < \gamma_2$, for any $x \in \mathcal{M}$,

$$\begin{cases} 0.9\|y - x\| \leq 0.9d_{\mathcal{M}}(x, y) \leq \|u\|_{\mathbb{R}^d} \leq \|y - x\| \leq d_{\mathcal{M}}(x, y), \\ \left| \det \left(\frac{dy}{du} \right) \right| \leq 2, \quad \|y - x\|^2 = \|u\|^2 + O_{MC}(\|u\|^4), \end{cases} \quad \forall y \in \mathcal{M} \cap B_{\delta_\gamma}(x). \quad (25)$$

This $\gamma_2(\mathcal{M})$ depends on manifold curvature, and is small when manifold curvature has large magnitude.

Set $\gamma_0 = \min\{\gamma_1, \gamma_2\}$, when $\gamma < \min\{\gamma_0, 1\}$, we have (24) and (25), where the big-O notation means that the corresponding term has absolute value bounded by the implied constant times the quantity inside the $O(\cdot)$.

We now expand f locally at x , and we separate the two cases, $\beta \leq 1$, and $1 < \beta \leq 2$.

Case 1: $\beta \leq 1$.

Let $y \in B_{\delta_\gamma}(x) \cap \mathcal{M}$, because f has Hölder constant L_f , $|f(y) - f(x)| \leq L_f d_{\mathcal{M}}(x, y)^\beta$. By (25), and that $0 < \beta \leq 1$, $d_{\mathcal{M}}(x, y)^\beta \leq \frac{\|u\|^\beta}{0.9^\beta} \leq 0.9^{-1} \|u\|^\beta$. Thus, with absolute constant in big-O,

$$f(y) = f(x) + O(L_f \|u\|^\beta), \quad \forall y \in \mathcal{M} \cap B_{\delta_\gamma}(x). \quad (26)$$

Meanwhile, by (25) and that h is C^1 on $(0, \infty)$,

$$h\left(\frac{\|x-y\|^2}{\gamma^2}\right) = h\left(\frac{\|u\|^2 + O_{MC}(\|u\|^4)}{\gamma^2}\right) = h\left(\frac{\|u\|^2}{\gamma^2}\right) + h'(\xi(u)) O_{MC}\left(\frac{\|u\|^4}{\gamma^2}\right),$$

where $\xi(u)$ is between $\frac{\|u\|^2}{\gamma^2}$ and $\frac{\|x-y\|^2}{\gamma^2}$. By (25), $\xi(u) \geq \frac{\|u\|^2}{\gamma^2}$, and then by Assumption 3.3(C2),

$$|h'(\xi(u))| \leq a_1 e^{-a \frac{\|u\|^2}{\gamma^2}}. \quad (27)$$

Then, we define $B'_x := \phi_x(\mathcal{M} \cap B_{\delta_\gamma}(x)) \subset \mathbb{R}^d$ and have that

$$\begin{aligned}
& \gamma^{-d} \int_{\mathcal{M} \cap B_{\delta_\gamma}(x)} h \left(\frac{\|x-y\|^2}{\gamma^2} \right) f(y) dV(y) \\
&= \gamma^{-d} \int_{B'_x} \left(h \left(\frac{\|u\|^2}{\gamma^2} \right) + a_1 e^{-a \frac{\|u\|^2}{\gamma^2}} O_{MC} \left(\frac{\|u\|^4}{\gamma^2} \right) \right) f(y(u)) \left| \det \left(\frac{dy}{du} \right) \right| du \\
&= \gamma^{-d} \int_{B'_x} h \left(\frac{\|u\|^2}{\gamma^2} \right) (f(x) + O(L_f \|u\|^\beta)) \left| \det \left(\frac{dy}{du} \right) \right| du \\
&\quad + \gamma^{-d} \int_{B'_x} a_1 e^{-a \frac{\|u\|^2}{\gamma^2}} O_{MC} \left(\frac{\|u\|^4}{\gamma^2} \right) \|f\|_\infty \left| \det \left(\frac{dy}{du} \right) \right| du = \textcircled{1} + \textcircled{2} + \textcircled{3},
\end{aligned} \tag{28}$$

where, by (24),

$$\textcircled{1} := f(x) \gamma^{-d} \int_{B'_x} h \left(\frac{\|u\|^2}{\gamma^2} \right) (1 + O_{MC}(\|u\|^2)) du,$$

and by (25), $\left| \det \left(\frac{dy}{du} \right) \right| \leq 2$,

$$\textcircled{2} := \gamma^{-d} \int_{B'_x} h \left(\frac{\|u\|^2}{\gamma^2} \right) O(L_f \|u\|^\beta) 2 du,$$

$$\textcircled{3} := \gamma^{-d} \int_{B'_x} a_1 e^{-a \frac{\|u\|^2}{\gamma^2}} O_{MC} \left(\frac{\|u\|^4}{\gamma^2} \right) \|f\|_\infty 2 du.$$

To proceed, note that B'_x is not a ball on \mathbb{R}^d but is contained between two spheres: by (25), we have $B_{0.9\delta_\gamma}^d(0) \subset B'_x \subset B_{\delta_\gamma}^d(0)$. This together with the exponential decay of h gives that

$$\begin{aligned}
& \left| \gamma^{-d} \int_{B'_x} h \left(\frac{\|u\|^2}{\gamma^2} \right) du - m_0 \right| \leq \left| \gamma^{-d} \int_{\mathbb{R}^d \setminus B_{0.9\delta_\gamma}^d(0)} h \left(\frac{\|u\|^2}{\gamma^2} \right) du \right| \\
& \leq \int_{v \in \mathbb{R}^d, \|v\| \geq 0.9\delta_\gamma/\gamma} e^{-a\|v\|^2} dv = O_{GM,a}(\gamma^{10}).
\end{aligned}$$

Meanwhile, $\gamma^{-d} \int_{B'_x} h \left(\frac{\|u\|^2}{\gamma^2} \right) \|u\|^2 du = O_{GM,a}(\gamma^2)$. Thus,

$$\textcircled{1} = f(x)(m_0[h] + O_{GM,a}(\gamma^{10}) + O_{GM,a,MC}(\gamma^2)) = m_0 f(x) + O_{GM,a,MC}(\|f\|_\infty \gamma^2).$$

Similarly, $\gamma^{-d} \int_{B'_x} h \left(\frac{\|u\|^2}{\gamma^2} \right) \|u\|^\beta du = O_{GM,a}(\gamma^\beta)$, and then

$$\textcircled{2} = O_{GM,a}(L_f \gamma^\beta).$$

Finally, $\gamma^{-d} \int_{B'_x} e^{-a \frac{\|u\|^2}{\gamma^2}} \frac{\|u\|^4}{\gamma^2} du = O_{GM,a}(\gamma^2)$, and then

$$\textcircled{3} = O_{GM,a,a_1,MC}(\|f\|_\infty \gamma^2).$$

Putting together, we have that (28) equals

$$\textcircled{1} + \textcircled{2} + \textcircled{3} = m_0[h]f(x) + O_{GM,a,a_1,MC}(\|f\|_\infty \gamma^2) + O_{GM,a}(L_f \gamma^\beta),$$

and the integral outside $B_{\delta_\gamma}(x)$ gives $O_{MV}(\|f\|_\infty \gamma^{10})$ as shown in (23). Because $\gamma < 1$, $\gamma^{10} \leq \gamma^2$. Combined together, this proves (8) under case 1 with C_1 being some $C_1^{(\text{case 1})}$, which depends on h (including

constants a, a_1), d , and manifold curvature and volume.

Case 2: $1 < \beta \leq 2$.

Recall the definition of Hölder constant L_f when $\beta > 1$, the expansion (26) has the the following counterpart for any $y \in \mathcal{M} \cap B_{\delta_\gamma}(x)$,

$$\begin{aligned} f(y) &= f(x) + \nabla_{\mathcal{M}} f(x)^T (u + O_{MC}(\|u\|^2) + O(L_f \|u\|^\beta)) \\ &= f(x) + \nabla_{\mathcal{M}} f(x)^T u + O_{MC}(L_f \|u\|^\beta). \end{aligned} \quad (29)$$

Then similarly expanding the kernel $h(\frac{\|x-y\|^2}{\gamma^2})$ in the integral, we have

$$\gamma^{-d} \int_{\mathcal{M} \cap B_{\delta_\gamma}(x)} h\left(\frac{\|x-y\|^2}{\gamma^2}\right) f(y) dV(y) = \textcircled{1} + \textcircled{2} + \textcircled{3},$$

where

$$\textcircled{1} := \gamma^{-d} \int_{B'_x} h\left(\frac{\|u\|^2}{\gamma^2}\right) (f(x) + \nabla_{\mathcal{M}} f(x)^T u) (1 + O_{MC}(\|u\|^2)) du,$$

and again, since $\left| \det\left(\frac{dy}{du}\right) \right| \leq 2$,

$$\textcircled{2} := \gamma^{-d} \int_{B'_x} h\left(\frac{\|u\|^2}{\gamma^2}\right) O_{MC}(L_f \|u\|^\beta) 2 du,$$

$$\textcircled{3} := \gamma^{-d} \int_{B'_x} a_1 e^{-a \frac{\|u\|^2}{\gamma^2}} O_{MC}\left(\frac{\|u\|^4}{\gamma^2}\right) \|f\|_\infty 2 du.$$

Same as before, $\textcircled{3} = O_{GM,a,a_1,MC}(\|f\|_\infty \gamma^2)$, and $\textcircled{2} = O_{GM,a,MC}(L_f \gamma^\beta)$. Also, $\textcircled{1} = \textcircled{4} + \textcircled{5}$, where

$$\begin{aligned} \textcircled{4} &= \gamma^{-d} \int_{B'_x} h\left(\frac{\|u\|^2}{\gamma^2}\right) (f(x) + \nabla_{\mathcal{M}} f(x)^T u) du \\ &= m_0 f(x) + f(x) O_{GM,a}(\gamma^{10}) + 0 + \|\nabla_{\mathcal{M}} f(x)\| O_{GM,a}(\gamma^{10}) \\ &= m_0 f(x) + O_{GM,a}(\|f\|_\infty + \|\nabla_{\mathcal{M}} f(x)\|) \gamma^{10}, \end{aligned}$$

where in the 2nd equality we used that the integral of $h(\frac{\|u\|^2}{\gamma^2}) u du$ vanishes on \mathbb{R}^d ;

$$\begin{aligned} \textcircled{5} &= \gamma^{-d} \int_{B'_x} h\left(\frac{\|u\|^2}{\gamma^2}\right) (f(x) + \nabla_{\mathcal{M}} f(x)^T u) O_{MC}(\|u\|^2) du \\ &= O_{MC,GM,a}(\|f\|_\infty \gamma^2) + O_{MC,GM,a}(\|\nabla_{\mathcal{M}} f\|_\infty \gamma^3). \end{aligned}$$

Putting together, by that $\|\nabla_{\mathcal{M}} f\|_\infty \leq L_f$, we have

$$\textcircled{1} = m_0 [h] f(x) + O_{MC,GM,a}(\|f\|_\infty \gamma^2) + O_{MC,GM,a}(L_f \gamma^3),$$

and thus, since $\gamma^3 \leq \gamma^\beta$,

$$\textcircled{1} + \textcircled{2} + \textcircled{3} = m_0 [h] f(x) + O_{GM,a,MC}(L_f \gamma^\beta) + O_{GM,a,a_1,MC}(\|f\|_\infty \gamma^2).$$

The integral outside $B_{\delta_\gamma}(x)$ again can be incorporated into the residual term above because $\gamma^{10} \leq \gamma^2$. This proves (8) under case 2 with C_1 being some $C_1^{(\text{case 2})}$ which depends on the kernel function h , d , and manifold curvature and volume.

Choosing $C_1 = \max\{C_1^{(\text{case 1})}, C_1^{(\text{case 2})}\}$ makes (8) hold for both cases. \square

Proof of Lemma 3.2. By Lemma 3.1, we have that when $\gamma < \min\{\gamma_0, 1\}$,

$$\begin{aligned}\mathbb{E}_{x \sim p, y \sim p} K_\gamma(x, y) &= \int_{\mathcal{M}} p(x) \left(\int_{\mathcal{M}} K_\gamma(x, y) p(y) dV(y) \right) dV(x) \\ &= \int_{\mathcal{M}} p(x) \gamma^d (m_0 p(x) + r_1(x)) dV(x), \quad \|r_1\|_\infty \leq C_1(L_\rho \gamma^\beta + \rho_{\max} \gamma^2) \\ &= \gamma^d \left(m_0 [h] \int_{\mathcal{M}} p^2 + s_1 \right), \quad |s_1| \leq C_1(L_\rho \gamma^\beta + \rho_{\max} \gamma^2),\end{aligned}\tag{30}$$

where we use the short-handed notation $\int_{\mathcal{M}} p^2 = \int_{\mathcal{M}} p(x)^2 dV(x)$. Similarly,

$$\begin{aligned}\mathbb{E}_{x \sim q, y \sim q} K_\gamma(x, y) &= \gamma^d \left(m_0 [h] \int_{\mathcal{M}} q^2 + s_2 \right), \\ \mathbb{E}_{x \sim p, y \sim q} K_\gamma(x, y) &= \gamma^d \left(m_0 [h] \int_{\mathcal{M}} pq + s_3 \right), \\ |s_2|, |s_3| &\leq C_1(L_\rho \gamma^\beta + \rho_{\max} \gamma^2),\end{aligned}\tag{31}$$

Thus, by definition of T ,

$$T = \gamma^d \left(m_0 [h] \int_{\mathcal{M}} (p - q)^2 + s_1 + s_2 - 2s_3 \right),$$

which proves (10) by the bounds of $|s_1|, |s_2|, |s_3|$ in (30) and (31). \square

Proof of Prop. 3.4. By definition,

$$\widehat{T} = \widehat{T}_{XX} + \widehat{T}_{YY} - 2\widehat{T}_{XY},$$

where

$$\widehat{T}_{XX} = \frac{1}{n_X^2} \sum_{i, i'=1} K_\gamma(x_i, x_{i'}), \quad \widehat{T}_{YY} = \frac{1}{n_Y^2} \sum_{j, j'=1} K_\gamma(y_j, y_{j'}), \quad \widehat{T}_{XY} = \frac{1}{n_X n_Y} \sum_{i, j} K_\gamma(x_i, y_j),$$

and we analyze the concentration of the three terms respectively. By (11),

$$n_X - 1 \geq 0.9\rho_X n, \quad n_Y - 1 \geq 0.9(1 - \rho_X)n,$$

and thus by definition of c as in (12),

$$cn \leq n_X - 1, \quad n_Y - 1 \leq n.\tag{32}$$

We first analyze \widehat{T}_{XX} . Since $K_\gamma(x, x) = h(0) = 1$,

$$\widehat{T}_{XX} = \frac{1}{n_X} + \left(1 - \frac{1}{n_X}\right) V_{XX}, \quad V_{XX} := \frac{1}{n_X(n_X - 1)} \sum_{i \neq j, i, j=1}^{n_X} K_\gamma(x_i, x_j).$$

We write $n_X = N$ for a short-handed notation. Define, for $i \neq j$, $V_{i,j} := K_\gamma(x_i, x_j)$, we have that

$$\mathbb{E}V_{i,j} = \mathbb{E}_{x \sim p, y \sim p} K_\gamma(x, y).$$

Meanwhile, by that $|h(r)| \leq 1 := L_V$ for any $r \in [0, \infty)$, due to Assumption 3.3 (C2), we always have $|V_{i,j}| \leq 1$. The variance

$$\text{Var}(V_{i,j}) \leq \mathbb{E}V_{i,j}^2 = \int_{\mathcal{M}} \int_{\mathcal{M}} h^2 \left(\frac{\|x - y\|^2}{\gamma^2} \right) p(x)p(y) dV(x) dV(y).$$

Note that $h_2 := h^2$ also satisfies Assumption 3.3 (with constants a replaced $2a$, same $a_0 = 1$ and a_1 replaced by $2a_1$), and thus one can apply Lemma 3.1 with h replace by h_2 , which does not change the threshold constant γ_0 , but the constant C_1 in the error bound changes to $C_1^{(2)}$ corresponding to the new kernel function h_2 . Since $\gamma < \min\{1, \gamma_0\}$, applying Lemma 3.1 with h_2 and $f = 1$ gives that

$$\left| \gamma^{-d} \int_{\mathcal{M}} h^2 \left(\frac{\|x - y\|^2}{\gamma^2} \right) dV(y) - m_0[h^2] \right| \leq C_1^{(2)} \gamma^2.$$

Thus

$$\begin{aligned} \mathbb{E}V_{ij}^2 &\leq \gamma^d \|p\|_\infty \int_{\mathcal{M}} p(x) \left(m_0[h^2] + C_1^{(2)} \gamma^2 \right) dV(x) \\ &\leq \gamma^d \rho_{\max} \left(m_0[h^2] + C_1^{(2)} \gamma^2 \right), \end{aligned} \quad (33)$$

Since we assume $\gamma < \frac{1}{\sqrt{C_1^{(2)}}}$ in the condition, by definition of ν as in (12), we then have that

$$\text{Var}(V_{ij}) \leq \gamma^d \nu. \quad (34)$$

We use the decoupling of U-statistics: Define $\tilde{V}_{i,j} = V_{i,j} - \mathbb{E}V_{i,j}$ for $i \neq j$. For any $s > 0$, let \mathcal{S}_N be denote the permutation group of N elements, we have

$$\begin{aligned} V_{XX} &= \frac{1}{N(N-1)} \sum_{i \neq j} \tilde{V}_{i,j} = \frac{1}{N!} \frac{1}{N(N-1)} \sum_{\gamma \in \mathcal{S}_N} \sum_{i \neq j} \tilde{V}_{\gamma(i), \gamma(j)} \\ &= \frac{1}{N!} \frac{1}{\lfloor N/2 \rfloor} \sum_{\gamma \in \mathcal{S}_N} \sum_{i=1}^{\lfloor N/2 \rfloor} \tilde{V}_{\gamma(2i-1), \gamma(2i)}. \end{aligned}$$

Then, by Jensen's inequality, let $M = \lfloor N/2 \rfloor$,

$$\mathbb{E}e^{sV_{XX}} \leq \frac{1}{N!} \sum_{\gamma \in \mathcal{S}_N} \mathbb{E} \exp \left\{ s \frac{1}{M} \sum_{i=1}^M \tilde{V}_{\gamma(2-i), \gamma(2i)} \right\} = \mathbb{E} \exp \left\{ s \frac{1}{M} \sum_{i=1}^M \tilde{V}_{2i-1, 2i} \right\},$$

and the sum over i is an independent sum over M random variables. By that $|\tilde{V}_{ij}| \leq 1$, and (34), then same as in the derivation of the classical Bernstein's inequality, we have that for any $t > 0$,

$$\mathbb{P}[V_{XX} - \mathbb{E}V_{ij} > t] \leq \exp \left\{ -\frac{\lfloor N/2 \rfloor t^2}{2\gamma^d \nu + \frac{2}{3} t L_V} \right\} \leq \exp \left\{ -\frac{(N-1)t^2}{2(2\gamma^d \nu + \frac{2}{3} t L_V)} \right\}.$$

We target at

$$t = \lambda \sqrt{\frac{\gamma^d \nu}{N-1}}, \quad \lambda > 0,$$

and when

$$\frac{t L_V}{3} < \gamma^d \nu, \quad (35)$$

the tail probability is bounded by

$$\exp \left\{ -\frac{(N-1)t^2}{8\gamma^d \nu} \right\} = \exp \left\{ -\frac{\lambda^2}{8} \right\}.$$

By that $L_V = 1$, (35) is equivalent to $\lambda\sqrt{\frac{\gamma^{d\nu}}{N-1}} < 3\gamma^{d\nu}$ which is

$$0 < \lambda < 3\sqrt{\nu\gamma^d(N-1)}.$$

This proves that

$$\mathbb{P}\left[V_{XX} - \mathbb{E}V_{ij} > \lambda\sqrt{\frac{\gamma^{d\nu}}{N-1}}\right] \leq e^{-\lambda^2/8}, \quad \forall 0 < \lambda < 3\sqrt{\nu\gamma^d(N-1)}. \quad (36)$$

The low-tail can be proved similarly, so we have

$$\mathbb{P}\left[V_{XX} - \mathbb{E}_{x\sim p, y\sim p}K_\gamma(x, y) > \lambda\sqrt{\frac{\gamma^{d\nu}}{n_X-1}}\right] \leq e^{-\lambda^2/8}, \quad \forall 0 < \lambda < 3\sqrt{\nu\gamma^d(n_X-1)}, \quad (37)$$

and same for $\mathbb{P}\left[V_{XX} - \mathbb{E}_{x\sim p, y\sim p}K_\gamma(x, y) < -\lambda\sqrt{\frac{\gamma^{d\nu}}{n_X-1}}\right]$.

Similarly, we have

$$\widehat{T}_{YY} = \frac{1}{n_Y} + (1 - \frac{1}{n_Y})V_{YY}, \quad V_{YY} := \frac{1}{n_Y(n_Y-1)} \sum_{i \neq j, i, j=1}^{n_Y} K_\gamma(y_i, y_j).$$

and

$$\mathbb{P}\left[V_{YY} - \mathbb{E}_{x\sim q, y\sim q}K_\gamma(x, y) > \lambda\sqrt{\frac{\gamma^{d\nu}}{n_Y-1}}\right] \leq e^{-\lambda^2/8}, \quad \forall 0 < \lambda < 3\sqrt{\nu\gamma^d(n_Y-1)}, \quad (38)$$

and same for $\mathbb{P}\left[V_{YY} - \mathbb{E}_{x\sim q, y\sim q}K_\gamma(x, y) < -\lambda\sqrt{\frac{\gamma^{d\nu}}{n_Y-1}}\right]$.

To analyze \widehat{T}_{XY} , define $M := \min\{n_X, n_Y\}$, and

$$\tilde{V}_{i,j} = K_\gamma(x_i, y_j) - \mathbb{E}_{x\sim p, y\sim q}K_\gamma(x, y), \quad i = 1, \dots, n_X, y = 1, \dots, n_Y.$$

Then for any $s > 0$, let \mathcal{S}_X and \mathcal{S}_Y denote the permutation group of n_X and n_Y elements respectively, we then have

$$\begin{aligned} \frac{1}{n_X n_Y} \sum_{i=1}^{n_X} \sum_{j=1}^{n_Y} \tilde{V}_{i,j} &= \frac{1}{n_X!} \frac{1}{n_Y!} \frac{1}{n_X n_Y} \sum_{\gamma_X \in \mathcal{S}_X} \sum_{\gamma_Y \in \mathcal{S}_Y} \sum_{i=1}^{n_X} \sum_{j=1}^{n_Y} \tilde{V}_{\gamma_X(i), \gamma_Y(j)} \\ &= \frac{1}{n_X!} \frac{1}{n_Y!} \frac{1}{M} \sum_{\gamma_X \in \mathcal{S}_X} \sum_{\gamma_Y \in \mathcal{S}_Y} \sum_{i=1}^M \tilde{V}_{\gamma_X(i), \gamma_Y(i)}. \end{aligned}$$

Then, by Jensen's inequality,

$$\begin{aligned} \mathbb{E} \exp \left\{ s \frac{1}{n_X n_Y} \sum_{i=1}^{n_X} \sum_{j=1}^{n_Y} \tilde{V}_{i,j} \right\} &\leq \frac{1}{n_X!} \frac{1}{n_Y!} \sum_{\gamma_X \in \mathcal{S}_X} \sum_{\gamma_Y \in \mathcal{S}_Y} \mathbb{E} \exp \left\{ s \frac{1}{M} \sum_{i=1}^M \tilde{V}_{\gamma_X(i), \gamma_Y(i)} \right\} \\ &= \mathbb{E} \exp \left\{ s \frac{1}{M} \sum_{i=1}^M \tilde{V}_{i,i} \right\}, \end{aligned}$$

and $\tilde{V}_{i,i} = K_\gamma(x_i, y_i) - \mathbb{E}K_\gamma(x_i, y_i)$ across $i = 1, \dots, M$ are independent. By that $|\tilde{V}_{ij}| \leq 1$, and same as before, by applying Lemma 3.1 with h^2 and use that $\gamma < \frac{1}{\sqrt{C_1^{(2)}}}$,

$$\text{Var}(\tilde{V}_{ij}) \leq \mathbb{E}V_{ij}^2 = \int_{\mathcal{M}} \int_{\mathcal{M}} h^2 \left(\frac{\|x - y\|^2}{\gamma^2} \right) p(x)q(y) dV(x)dV(y) \leq \gamma^d \nu,$$

then same as in proving (36), we have

$$\mathbb{P} \left[\hat{T}_{XY} - \mathbb{E}_{x \sim p, y \sim q} K_\gamma(x, y) > \lambda \sqrt{\frac{\gamma^d \nu}{M}} \right] \leq e^{-\lambda^2/8}, \quad \forall 0 < \lambda < 3\sqrt{\nu \gamma^d M}, \quad (39)$$

and same for $\mathbb{P} \left[\hat{T}_{XY} - \mathbb{E}_{x \sim p, y \sim q} K_\gamma(x, y) < -\lambda \sqrt{\frac{\gamma^d \nu}{M}} \right]$.

Recall that

$$\hat{T} = (V_{XX} + V_{YY} - 2\hat{T}_{XY}) + \frac{1}{n_X}(1 - V_{XX}) + \frac{1}{n_Y}(1 - V_{YY}),$$

we now collect (37), (38), (39) to derive concentration of \hat{T} under H_0 and H_1 respectively:

Under H_0 , we consider upperbound of \hat{T} . The uniform boundedness of $|h|$ by 1, by Assumption 3.3 (C2), implies that $|V_{XX}|, |V_{YY}| \leq 1$, and then

$$\hat{T} \leq (V_{XX} + V_{YY} - 2\hat{T}_{XY}) + 2\left(\frac{1}{n_X} + \frac{1}{n_Y}\right),$$

and thus, by that $n_X - 1, n_Y - 1 \geq cn$, for any $\lambda < 3\sqrt{c\nu\gamma^d n}$, w.p. $> 1 - 3e^{-\lambda^2/8}$,

$$\hat{T} \leq \frac{4}{cn} + 4\lambda \sqrt{\frac{\gamma^d \nu}{cn}},$$

because $(\mathbb{E}_{x \sim p, y \sim p} + \mathbb{E}_{x \sim q, y \sim q} - 2\mathbb{E}_{x \sim p, y \sim q})K_\gamma(x, y) = 0$ when $p = q$.

Under H_1 , because $1 - V_{XX}, 1 - V_{YY} \geq 0$,

$$\hat{T} \geq V_{XX} + V_{YY} - 2\hat{T}_{XY}.$$

By the definition of T and the concentration of V_{XX}, V_{YY} , and \hat{T}_{XY} as above, using $n_X, n_Y \geq cn$ again, we have that for any $\lambda < 3\sqrt{c\nu\gamma^d n}$, w.p. $\geq 1 - 3e^{-\lambda^2/8}$,

$$\hat{T} \geq T - 4\lambda \sqrt{\frac{\gamma^d \nu}{cn}}.$$

□

Proof of Theorem 3.5. Under the condition of the theorem, the conditions needed by Proposition 3.4 and Lemma 3.2 are both satisfied. We first verify that the Type-I error is at most α_{level} . The definition of λ_1 makes that $3e^{-\lambda_1^2/8} = \alpha_{\text{level}}$. By the definition of t_{thres} and Proposition 3.4(1), the type-I error bound holds as long as $\lambda_1 < 3\sqrt{c\nu\gamma^d n}$, and this is guaranteed by (14).

Next we address the Type-II error. By Proposition 3.4(2), the bound $e^{-\lambda_2^2/8}$ holds as long as $\lambda_2 < 3\sqrt{c\nu\gamma^d n}$ and

$$t_{\text{thres}} < T - 4\lambda_2 \sqrt{\frac{\nu \gamma^d}{c n}}. \quad (40)$$

By Lemma 3.2, $T = \gamma^d(D_{p,q} + r_T)$, and $|r_T| \leq 4C_1(L_\rho \gamma^\beta + \rho_{\max} \gamma^2)$. By (13), we have

$$|r_T| < 0.1D_{p,q},$$

and then $T > \gamma^d 0.9 D_{p,q}$. Meanwhile, (14) gives that

$$\frac{4}{cn} < 0.4\gamma^d D_{p,q}, \quad 4(\lambda_1 + \lambda_2)\sqrt{\frac{\nu}{c}\frac{\gamma^d}{n}} < 0.5\gamma^d D_{p,q}. \quad (41)$$

Thus, $\frac{4}{cn} + 4(\lambda_1 + \lambda_2)\sqrt{\frac{\nu}{c}\frac{\gamma^d}{n}} < 0.9\gamma^d D_{p,q} < T$, which implies (40) by the constructive choice of t_{thres} here. \square

7.2 Proofs in Section 4.1

Proof of Lemma 4.1. The proof uses same technique as Lemma 3.1 and the handling of x near boundary follows the method of Lemma 9 in [18].

The constant γ'_0 is defined similarly as before, to guarantee the existence of local chart at point x both away from and near boundary (including the uniqueness of the Euclidean distance nearest point $x_0 \in \partial\mathcal{M}$ to each x when $d_E(x, \partial\mathcal{M}) \leq \delta_\gamma$), along with the local metric and volume comparison after using projected coordinates u as (24) and (25). The existence of such γ'_0 is due to compactness of \mathcal{M} . By truncating the integral of $dV(y)$ on $B_{\delta_\gamma}(x) \cap \mathcal{M}$ same as before, when $d_E(x, \partial\mathcal{M}) > \delta_\gamma$, the claim follows the proof of Lemma 3.1 with the constant C_1 be some $C'_{1,\text{interior}}$.

To analyze the case for x where $d_E(x, \partial\mathcal{M}) \leq \delta_\gamma$, let $x_0 \in \partial\mathcal{M}$ be the nearest point on the boundary to x under Euclidean distance, and we follow the same change of coordinates around x_0 as in the proof of Lemma 9 in [18]. By the symmetry of the kernel $h(\frac{\|u\|^2}{\gamma^2})$ and the same analysis in Lemma 9 of [18], one can show that

$$\begin{aligned} \gamma^{-d} \int_{B_{\delta_\gamma}(x) \cap \mathcal{M}} h\left(\frac{\|x-y\|^2}{\gamma^2}\right) f(y) dV(y) &= f(x) m_0^{(\gamma)}[h](x) + O_{GM,a}(L_f \gamma^\beta) \\ &\quad + O_{GM,a,a_1,MC}(\|f\|_\infty \gamma^2), \end{aligned}$$

where $m_0^{(\gamma)}[h](x)$ equals the integral of $\gamma^{-d} h(\frac{\|u\|^2}{\gamma^2})$ on a partial domain in \mathbb{R}^d and the domain depends on the location of x , defined in the same way as in Lemma 9 in [18], and it satisfies that $m_0^{(\gamma)}[h](x) \leq m_0[h]$ due to that $h \geq 0$ by Assumption 3.3 (C3). The $O_{GM,a}(L_f \gamma^\beta)$ term is due to the expansion of f near x , and the $O_{GM,a,a_1,MC}(\|f\|_\infty \gamma^2)$ due to the expansion of kernel and the volume form $|\det(\frac{dy}{du})| = 1 + O(\|u\|^2)$, similar as in the proof of Lemma 3.1. Putting together, this proves (17) with the bound $C'_{1,\text{boundary}}(L_f \gamma^\beta + \|f\|_\infty \gamma^2)$ on the r.h.s.

Taking $C' = \max\{C'_{1,\text{interior}}, C'_{1,\text{boundary}}\}$ finishes the proof of the lemma. \square

Proof of Lemma 4.2. The constant δ_γ as in Lemma 4.1. By Lemma 4.1, when $\gamma < \min\{\gamma'_0, 1\}$, define $P_\gamma := \{x \in \mathcal{M}, d_E(x, \partial\mathcal{M}) \leq \delta_\gamma\}$ which is the near-boundary set, we have that

$$\begin{aligned} \mathbb{E}_{x \sim p, y \sim p} K_\gamma(x, y) &= \int_{\mathcal{M}} p(x) \left(\int_{\mathcal{M}} K_\gamma(x, y) p(y) dV(y) \right) dV(x) \\ &= \int_{\mathcal{M} \setminus P_\gamma} p(x) \gamma^d (m_0[h] p(x) + r_1(x)) dV(x) \\ &\quad + \int_{P_\gamma} p(x) \gamma^d (m_0^{(\gamma)}[h](x) p(x) + r_1(x)) dV(x) \\ &= \gamma^d \left(\int_{\mathcal{M} \setminus P_\gamma} m_0[h] p(x)^2 dV(x) \right. \\ &\quad \left. + \int_{P_\gamma} m_0^{(\gamma)}[h](x) p(x)^2 dV(x) + \int_{\mathcal{M}} p(x) r_1(x) dV(x) \right), \end{aligned} \quad (42)$$

where

$$\|r_1\|_\infty \leq C'_1(L_\rho\gamma^\beta + \rho_{\max}\gamma^2).$$

Note that

$$\begin{aligned} & \left| m_0[h] \int_{\mathcal{M} \setminus P_\gamma} p^2 + \int_{P_\gamma} m_0^{(\gamma)}[h](x)p(x)^2 dV(x) - m_0[h] \int_{\mathcal{M}} p^2 \right| \\ &= \left| \int_{P_\gamma} (m_0^{(\gamma)}[h](x) - m_0[h])p(x)^2 dV(x) \right| \leq \int_{P_\gamma} |m_0^{(\gamma)}[h](x) - m_0[h]|p(x)^2 dV(x) \\ &\leq m_0[h] \int_{P_\gamma} p(x)^2 dV(x) \quad (\text{by that } 0 \leq m_0^{(\gamma)}[h](x) \leq m_0[h] \text{ for all } x \in P_\gamma) \\ &\leq m_0[h]\rho_{\max}^2 \int_{P_\gamma} dV(x), \end{aligned}$$

where the volume of the domain P_γ can be shown to be upper bounded by

$$\int_{P_\gamma} dV(x) \leq c_2\delta_\gamma|\partial\mathcal{M}|,$$

for some constant c_2 depending on the curvature of \mathcal{M} and the regularity of $\partial\mathcal{M}$. Back to (42), this gives that

$$\mathbb{E}_{x \sim p, y \sim p} K_\gamma(x, y) = \gamma^d \left(m_0[h] \int_{\mathcal{M}} p^2 + s'_1 + s_1 \right),$$

where

$$|s'_1| \leq m_0[h]c_2|\partial\mathcal{M}| \cdot \rho_{\max}^2\delta_\gamma, \quad |s_1| \leq C'_1(L_\rho\gamma^\beta + \rho_{\max}\gamma^2).$$

The computation of $\mathbb{E}_{x \sim q, y \sim q} K_\gamma(x, y)$ and $\mathbb{E}_{x \sim p, y \sim q} K_\gamma(x, y)$ are similar. Putting together as in the proof of Lemma 3.2, this proves (18) by the definition of δ_γ , with the constant C'_2 as stated. \square

- Proof of (19) when $\gamma < (C'_1)^{(2)}-1/2$

Proof of (19) . Similarly as in the proof of Proposition 3.4, by considering $h_2 = h^2$ as the kernel function,

$$\begin{aligned} \mathbb{E}_{x \sim p, y \sim p} K_\gamma(x, y)^2 &\leq \int_{\mathcal{M}} p(x)\rho_{\max} \left(\int_{\mathcal{M}} K_\gamma(x, y)^2 dV(y) \right) dV(x) \\ &= \rho_{\max}\gamma^d \left(\int_{\mathcal{M} \setminus P_\gamma} p(x)(m_0[h^2] + r_2(x))dV(x) \right. \\ &\quad \left. + \int_{P_\gamma} p(x)(m_0^{(\gamma)}[h^2](x) + r_2(x))dV(x) \right) \\ &\leq \rho_{\max}\gamma^d \left(\int_{\mathcal{M}} m_0[h^2]p(x)dV(x) + \int_{\mathcal{M}} p(x)|r_2(x)|dV(x) \right), \end{aligned} \tag{43}$$

where P_γ is as in the proof of Lemma 4.2, and the last inequality is by that $m_0^{(\gamma)}[h^2](x) \leq m_0[h^2]$. By applying Lemma 4.1 with h replaced by h^2 and $f = 1$, we have that for constant $C'_1{}^{(2)}$ which depends on (\mathcal{M}, h) , $C'_1{}^{(2)}$ corresponding to C'_1 in Lemma 4.1 with the kernel function h^2 ,

$$\|r_2\|_\infty \leq C'_1{}^{(2)}\gamma^2.$$

Thus,

$$\mathbb{E}_{x \sim p, y \sim p} K_\gamma(x, y)^2 \leq \gamma^d \rho_{\max} \left(m_0[h^2] + C'_1{}^{(2)}\gamma^2 \right)$$

which is bounded by $\gamma^d\nu$ when $C'_1{}^{(2)}\gamma^2 < 1$. \square

7.3 Proofs in Section 4.2

Recall that with Gaussian additive noise in \mathbb{R}^m , the law of x_i and y_i can be written as, for $k = 1, 2$,

$$x_i = x_i^{(c)} + \xi_i^{(1)}, \quad y_j = y_j^{(c)} + \xi_j^{(2)}, \quad x_i^{(c)} \sim p_{\mathcal{M}}, \quad y_j^{(c)} \sim q_{\mathcal{M}}, \quad \xi_i^{(k)} \sim \mathcal{N}(0, \sigma_{(k)}^2 I_m),$$

where $x_i^{(c)}$, $y_j^{(c)}$, $\xi_i^{(1)}$ and $\xi_i^{(2)}$ are independent, and $p_{\mathcal{M}}$ and $q_{\mathcal{M}}$ are manifold data densities supported on \mathcal{M} and satisfy Assumption 3.2. We want to show that our theory in Section 3 extends to this case when h is Gaussian kernel and the noise level $\sigma := \sqrt{\sigma_{(1)}^2 + \sigma_{(2)}^2} \leq \frac{c}{\sqrt{m}}\gamma$ for some constant c .

Though p and q are now supported on the ambient space, by the form of p and q and $h(\xi) = e^{-\xi/2}$, we have that

$$\begin{aligned} & \int_{\mathbb{R}^m} \int_{\mathbb{R}^m} K_{\gamma}(x, y) p(x) p(y) dx dy \\ &= \int_{\mathcal{M}} \int_{\mathcal{M}} \mathbb{E}_{\xi, \eta} \exp \left\{ -\frac{\|(x_1 + \xi) - (y_1 + \eta)\|^2}{2\gamma^2} \right\} p_{\mathcal{M}}(x_1) p_{\mathcal{M}}(y_1) dx_1 dy_1 \\ &= \int_{\mathcal{M}} \int_{\mathcal{M}} \mathbb{E}_g \exp \left\{ -\frac{\|(x_1 - y_1)/\gamma + g\|^2}{2} \right\} p_{\mathcal{M}}(x_1) p_{\mathcal{M}}(y_1) dx_1 dy_1, \quad g \sim \mathcal{N} \left(0, \frac{\sigma^2}{\gamma^2} I_m \right). \end{aligned}$$

Define $\tilde{\sigma}^2 := \frac{\sigma^2}{\gamma^2}$, we have that for any vector $v \in \mathbb{R}^m$,

$$\mathbb{E}_g \exp \left\{ -\frac{\|v + g\|^2}{2} \right\} = \frac{1}{(1 + \tilde{\sigma}^2)^{m/2}} \exp \left\{ -\frac{\|v\|^2}{2(1 + \tilde{\sigma}^2)} \right\},$$

thus $\int_{\mathbb{R}^m} \int_{\mathbb{R}^m} K_{\gamma}(x, y) p(x) p(y) dx dy$ can be equivalently written as

$$\int_{\mathcal{M}} \int_{\mathcal{M}} \frac{1}{(1 + \tilde{\sigma}^2)^{m/2}} \exp \left\{ -\frac{\|x_1 - y_1\|^2}{2\gamma^2(1 + \tilde{\sigma}^2)} \right\} p_{\mathcal{M}}(x_1) p_{\mathcal{M}}(y_1) dx_1 dy_1. \quad (44)$$

Because $h(\xi)^2 = e^{-\xi}$, the integral of $K_{\gamma}(x, y)^2$ can be computed similarly and it gives

$$\begin{aligned} & \int_{\mathbb{R}^m} \int_{\mathbb{R}^m} K_{\gamma}(x, y)^2 p(x) p(y) dx dy \\ &= \int_{\mathcal{M}} \int_{\mathcal{M}} \mathbb{E}_{\xi, \eta} \exp \left\{ -\frac{\|(x_1 + \xi) - (y_1 + \eta)\|^2}{\gamma^2} \right\} p_{\mathcal{M}}(x_1) p_{\mathcal{M}}(y_1) dx_1 dy_1 \\ &= \int_{\mathcal{M}} \int_{\mathcal{M}} \frac{1}{(1 + 2\tilde{\sigma}^2)^{m/2}} \exp \left\{ -\frac{\|x_1 - y_1\|^2}{\gamma^2(1 + 2\tilde{\sigma}^2)} \right\} p_{\mathcal{M}}(x_1) p_{\mathcal{M}}(y_1) dx_1 dy_1. \end{aligned} \quad (45)$$

Since $\sigma \leq \frac{c}{\sqrt{m}}\gamma$, $\tilde{\sigma}^2 \leq \frac{1}{m}c^2$, and then $1 \leq (1 + \tilde{\sigma}^2)^{m/2} \leq (1 + \frac{c^2}{m})^{m/2} \leq \exp\{c^2/2\}$, which means that the normalizing constant in (44) is bounded to be $O(1)$ constant. The same holds for that normalizing constant in (45), namely $1 \leq (1 + 2\tilde{\sigma}^2)^{m/2} \leq \exp\{c^2\}$. This means that one can apply Lemma 3.1 to compute the integrals in (44) and (45), replacing the p and q in the lemma by $p_{\mathcal{M}}$ and $q_{\mathcal{M}}$ respectively. We define the new effective kernel bandwidths in the Gaussian kernel: $\tilde{\gamma}^{(1)} := \gamma\sqrt{1 + \tilde{\sigma}^2}$ for integral of $K_{\gamma}(x, y)$ and $\tilde{\gamma}^{(2)} := \gamma\sqrt{1 + 2\tilde{\sigma}^2}$ for that of $K_{\gamma}(x, y)^2$. Since $\tilde{\sigma}^2 \leq \frac{1}{m}c^2$, the ratios of $\tilde{\gamma}^{(1)}/\gamma$ and $\tilde{\gamma}^{(2)}/\gamma$ are bounded by absolute constants from above and below. When m is large, the ratios are bounded to be $1 + O(m^{-1})$.

This gives the approximate expression of T in Lemma 3.2 involving $D_{p_{\mathcal{M}}, q_{\mathcal{M}}}$, as well as the boundedness of variance of $K_{\gamma}(x_i, x_j)$ (and $K_{\gamma}(y_i, y_j)$, $K_{\gamma}(x_i, y_j)$) needed in Proposition 3.4, replacing p and q with $p_{\mathcal{M}}$ and $q_{\mathcal{M}}$, and γ with the new effective kernel bandwidths in the analysis. These replacements allows to prove the same result as in Theorem 3.5 (the constants L_{ρ} and ρ_{\max} are with respect to $p_{\mathcal{M}}$ and $q_{\mathcal{M}}$), where the constants in the bounds need to be adjusted by multiplying some absolute ones.

References

- [1] Miguel A Arcones and Evarist Gine. On the bootstrap of u and v statistics. *The Annals of Statistics*, pages 655–674, 1992.
- [2] Krishnakumar Balasubramanian, Tong Li, and Ming Yuan. On the optimality of kernel-embedding based goodness-of-fit tests. *J. Mach. Learn. Res.*, 22:1–1, 2021.
- [3] Mikhail Belkin and Partha Niyogi. Laplacian eigenmaps for dimensionality reduction and data representation. *Neural computation*, 15(6):1373–1396, 2003.
- [4] Mikhail Belkin and Partha Niyogi. Convergence of laplacian eigenmaps. In *Advances in Neural Information Processing Systems*, pages 129–136, 2007.
- [5] Bhaswar B Bhattacharya. Asymptotic distribution and detection thresholds for two-sample tests based on geometric graphs. *The Annals of Statistics*, 48(5):2879–2903, 2020.
- [6] Monowar H Bhuyan, Dhruba Kumar Bhattacharyya, and Jugal K Kalita. Network anomaly detection: methods, systems and tools. *Ieee communications surveys & tutorials*, 16(1):303–336, 2013.
- [7] Mikołaj Bińkowski, Danica J. Sutherland, Michael Arbel, and Arthur Gretton. Demystifying MMD GANs. In *International Conference on Learning Representations*, 2018.
- [8] Karsten M Borgwardt, Arthur Gretton, Malte J Rasch, Hans-Peter Kriegel, Bernhard Schölkopf, and Alex J Smola. Integrating structured biological data by kernel maximum mean discrepancy. *Bioinformatics*, 22(14):e49–e57, 2006.
- [9] Antoni Buades, Bartomeu Coll, and J-M Morel. A non-local algorithm for image denoising. In *2005 IEEE Computer Society Conference on Computer Vision and Pattern Recognition (CVPR'05)*, volume 2, pages 60–65. IEEE, 2005.
- [10] Yang Cao, Arkadi Nemirovski, Yao Xie, Vincent Guigues, and Anatoli Juditsky. Change detection via affine and quadratic detectors. *Electronic journal of statistics*, 12(1):1–57, 2018.
- [11] Varun Chandola, Arindam Banerjee, and Vipin Kumar. Anomaly detection: A survey. *ACM Comput. Surv.*, 41(3), July 2009.
- [12] Varun Chandola, Arindam Banerjee, and Vipin Kumar. Anomaly detection for discrete sequences: A survey. *IEEE transactions on knowledge and data engineering*, 24(5):823–839, 2010.
- [13] Hao Chen and Jerome H Friedman. A new graph-based two-sample test for multivariate and object data. *Journal of the American statistical association*, 112(517):397–409, 2017.
- [14] Xiuyuan Cheng, Alexander Cloninger, and Ronald R Coifman. Two-sample statistics based on anisotropic kernels. *Information and Inference: A Journal of the IMA*, 9(3):677–719, 2020.
- [15] Xiuyuan Cheng and Hau-Tieng Wu. Convergence of graph Laplacian with kNN self-tuned kernels. *Information and Inference: A Journal of the IMA*, 09 2021. iaab019.
- [16] Kacper Chwiałkowski, Heiko Strathmann, and Arthur Gretton. A kernel test of goodness of fit. *JMLR: Workshop and Conference Proceedings*, 2016.
- [17] Kacper P Chwiałkowski, Aaditya Ramdas, Dino Sejdinovic, and Arthur Gretton. Fast two-sample testing with analytic representations of probability measures. In *Advances in Neural Information Processing Systems*, pages 1981–1989, 2015.

- [18] Ronald R Coifman and Stéphane Lafon. Diffusion maps. *Applied and computational harmonic analysis*, 21(1):5–30, 2006.
- [19] Eustasio del Barrio, Juan A. Cuesta-Albertos, Carlos Matrán, and Jesús M. Rodríguez-Rodríguez. Tests of goodness of fit based on the l_2 -wasserstein distance. *Ann. Statist.*, 27(4):1230–1239, 08 1999.
- [20] Arthur Gretton, Karsten M. Borgwardt, Malte J. Rasch, Bernhard Schölkopf, and Alexander Smola. A kernel two-sample test. *J. Mach. Learn. Res.*, 13:723–773, March 2012.
- [21] Arthur Gretton, Karsten M Borgwardt, Malte J Rasch, Bernhard Schölkopf, and Alexander Smola. A kernel two-sample test. *Journal of Machine Learning Research*, 13(Mar):723–773, 2012.
- [22] Arthur Gretton, Kenji Fukumizu, Zaïd Harchaoui, and Bharath K. Sriperumbudur. A fast, consistent kernel two-sample test. In Y. Bengio, D. Schuurmans, J. D. Lafferty, C. K. I. Williams, and A. Culotta, editors, *Advances in Neural Information Processing Systems 22*, pages 673–681. Curran Associates, Inc., 2009.
- [23] Arthur Gretton, Dino Sejdinovic, Heiko Strathmann, Sivaraman Balakrishnan, Massimiliano Pontil, Kenji Fukumizu, and Bharath K. Sriperumbudur. Optimal kernel choice for large-scale two-sample tests. In F. Pereira, C. J. C. Burges, L. Bottou, and K. Q. Weinberger, editors, *Advances in Neural Information Processing Systems 25*, pages 1205–1213. Curran Associates, Inc., 2012.
- [24] László Györfi and Edward C. Van Der Meulen. *A Consistent Goodness of Fit Test Based on the Total Variation Distance*, pages 631–645. Springer Netherlands, Dordrecht, 1991.
- [25] Laleh Haghverdi, Florian Buettner, and Fabian J Theis. Diffusion maps for high-dimensional single-cell analysis of differentiation data. *Bioinformatics*, 31(18):2989–2998, 2015.
- [26] Matthias Hein, Jean-Yves Audibert, and Ulrike Von Luxburg. From graphs to manifolds—weak and strong pointwise consistency of graph laplacians. In *International Conference on Computational Learning Theory*, pages 470–485. Springer, 2005.
- [27] James J Higgins. Introduction to modern nonparametric statistics. 2003.
- [28] W Hoeffding. Probability inequalities for sums of bounded random variables. *Journal of the American Statistical Association*, 58:301, 1963.
- [29] Harold Hotelling. The generalization of student’s ratio. *Ann. Math. Statist.*, 2(3):360–378, 08 1931.
- [30] Wittawat Jitkrittum, Heishiro Kanagawa, and Bernhard Schölkopf. Testing goodness of fit of conditional density models with kernels. In *Conference on Uncertainty in Artificial Intelligence*, pages 221–230. PMLR, 2020.
- [31] Wittawat Jitkrittum, Zoltán Szabó, Kacper P Chwialkowski, and Arthur Gretton. Interpretable distribution features with maximum testing power. In *Advances in Neural Information Processing Systems*, pages 181–189, 2016.
- [32] Wittawat Jitkrittum, Wenkai Xu, Zoltán Szabó, Kenji Fukumizu, and Arthur Gretton. A linear-time kernel goodness-of-fit test. In *Advances in Neural Information Processing Systems*, pages 262–271, 2017.
- [33] Frank J. Massey Jr. The kolmogorov-smirnov test for goodness of fit. *Journal of the American Statistical Association*, 46(253):68–78, 1951.

- [34] Chun-Liang Li, Wei-Cheng Chang, Yu Cheng, Yiming Yang, and Barnabás Póczos. Mmd gan: Towards deeper understanding of moment matching network. In *Advances in Neural Information Processing Systems*, pages 2203–2213, 2017.
- [35] Tong Li and Ming Yuan. On the optimality of gaussian kernel based nonparametric tests against smooth alternatives. *arXiv preprint arXiv:1909.03302*, 2019.
- [36] James R Lloyd and Zoubin Ghahramani. Statistical model criticism using kernel two sample tests. In C. Cortes, N. D. Lawrence, D. D. Lee, M. Sugiyama, and R. Garnett, editors, *Advances in Neural Information Processing Systems 28*, pages 829–837. Curran Associates, Inc., 2015.
- [37] James R Lloyd and Zoubin Ghahramani. Statistical model criticism using kernel two sample tests. In *Advances in Neural Information Processing Systems*, pages 829–837, 2015.
- [38] David Lopez-Paz and Maxime Oquab. Revisiting classifier two-sample tests. In *International Conference on Learning Representations*, 2017.
- [39] Malte D Luecken and Fabian J Theis. Current best practices in single-cell rna-seq analysis: a tutorial. *Molecular systems biology*, 15(6):e8746, 2019.
- [40] Arkadas Ozakin and Alexander Gray. Submanifold density estimation. *Advances in Neural Information Processing Systems*, 22:1375–1382, 2009.
- [41] Gabriel Peyré. Manifold models for signals and images. *Computer vision and image understanding*, 113(2):249–260, 2009.
- [42] J. Pfanzagl and O. Sheynin. Studies in the history of probability and statistics XLIV A forerunner of the t-distribution. *Biometrika*, 83(4):891–898, 12 1996.
- [43] John W. Pratt and Jean D. Gibbons. *Kolmogorov-Smirnov Two-Sample Tests*, pages 318–344. Springer New York, New York, NY, 1981.
- [44] Aaditya Ramdas, Nicolas Garcia, and Marco Cuturi. On wasserstein two sample testing and related families of nonparametric tests, 2015.
- [45] Aaditya Ramdas, Sashank Jakkam Reddi, Barnabás Póczos, Aarti Singh, and Larry Wasserman. On the decreasing power of kernel and distance based nonparametric hypothesis tests in high dimensions. In *Twenty-Ninth AAAI Conference on Artificial Intelligence*, 2015.
- [46] Mark Sandler, Andrew Howard, Menglong Zhu, Andrey Zhmoginov, and Liang-Chieh Chen. Mobilenetv2: Inverted residuals and linear bottlenecks. In *Proceedings of the IEEE Conference on Computer Vision and Pattern Recognition*, pages 4510–4520, 2018.
- [47] Robert J Serfling. *Approximation theorems of mathematical statistics*, volume 162. John Wiley & Sons, 2009.
- [48] Alexander Shapiro, Yao Xie, and Rui Zhang. Goodness-of-fit tests on manifolds. *IEEE Transactions on Information Theory*, 67(4):2539–2553, 2021.
- [49] Amit Singer. From graph to manifold laplacian: The convergence rate. *Applied and Computational Harmonic Analysis*, 21(1):128–134, 2006.
- [50] Bharath K Sriperumbudur, Kenji Fukumizu, Arthur Gretton, Bernhard Schölkopf, Gert RG Lanckriet, et al. On the empirical estimation of integral probability metrics. *Electronic Journal of Statistics*, 6:1550–1599, 2012.

- [51] Dougal J Sutherland, Hsiao-Yu Tung, Heiko Strathmann, Soumyajit De, Aaditya Ramdas, Alex Smola, and Arthur Gretton. Generative models and model criticism via optimized maximum mean discrepancy. *arXiv preprint arXiv:1611.04488*, 2016.
- [52] Laurens Van Der Maaten. Accelerating t-sne using tree-based algorithms. *The Journal of Machine Learning Research*, 15(1):3221–3245, 2014.
- [53] Ulrike Von Luxburg, Mikhail Belkin, and Olivier Bousquet. Consistency of spectral clustering. *The Annals of Statistics*, pages 555–586, 2008.
- [54] Larry Wasserman. *All of nonparametric statistics*. Springer Science & Business Media, 2006.
- [55] Liyan Xie and Yao Xie. Sequential change detection by optimal weighted ℓ_2 divergence. *IEEE Journal on Selected Areas in Information Theory*, 2(2):747–761, 2021.
- [56] Yao Xie and David Siegmund. Sequential multi-sensor change-point detection. *The Annals of Statistics*, 41(2):670–692, Apr 2013.
- [57] Lihi Zelnik-Manor and Pietro Perona. Self-tuning spectral clustering. In *Advances in neural information processing systems*, pages 1601–1608, 2005.
- [58] Jun Zhao, Ariel Jaffe, Henry Li, Ofir Lindenbaum, Esen Sefik, Ruaidhrí Jackson, Xiuyuan Cheng, Richard A Flavell, and Yuval Kluger. Detection of differentially abundant cell subpopulations in scrna-seq data. *Proceedings of the National Academy of Sciences*, 118(22), 2021.
- [59] Wei Zhu, Qiang Qiu, Jiaji Huang, Robert Calderbank, Guillermo Sapiro, and Ingrid Daubechies. Ldmnet: Low dimensional manifold regularized neural networks. In *Proceedings of the IEEE Conference on Computer Vision and Pattern Recognition*, pages 2743–2751, 2018.

A Algorithm and bootstrap estimation of t_{thres}

In experiments of kernel two-sample tests, we use the vanilla $O(n^2)$ algorithm to construct the kernel matrix from datasets X and Y and then compute the value of \hat{T} . The summary of the algorithm is as follows

Input data: X and Y , each having n_X and n_Y samples

Parameters: kernel bandwidth γ , test threshold t_{thres} if available.

Step 1. Construct the n -by- n kernel matrix, $n = n_X + n_Y$,

$$K = \begin{bmatrix} K_{XX}, K_{XY} \\ K_{XY}^T, K_{YY} \end{bmatrix},$$

where $K_{XX} = (K_\gamma(x_i, x_j))_{1 \leq i, j \leq n_X}$, $K_{YY} = (K_\gamma(y_i, y_j))_{1 \leq i, j \leq n_Y}$, and $K_{XY} = (K_\gamma(x_i, y_j))_{1 \leq i \leq n_X, 1 \leq j \leq n_Y}$.

Step 2. Compute \hat{T} as defined in (2) from the kernel matrix K .

Step 3. If $\hat{T} < t_{\text{thres}}$, accept $H_0 : p = q$, otherwise, reject H_0 .

If the test threshold t_{thres} is not provided, we use the bootstrap procedure [1] (previously used in [21, 45]) to estimate it from data: Given the computed kernel matrix K , and target test level α_{level} ,

Step 4. Repeating $l = 1, \dots, n_{\text{boot}}$ times:

- Randomly permute the rows and columns of K simultaneously, obtain a matrix K_l
- Compute the statistic \widehat{T}_i from K_l , treating the first n_X rows and columns are from one dataset and the other n_Y rows and columns from another data set.

Step 5. From the empirical distribution of n_{boot} , evaluate the $(1 - \alpha_{\text{level}})$ -quantile as t_{thres} .

Note that in the bootstrap procedure for threshold evaluation, no re-computing of the kernel matrix K is needed, but only the block average over the n^2 entries according to the permuted two sample class labels.

The testing power is estimated by n_{run} random replicas of the experiments and count the frequency that the test is corrected rejected when $q \neq p$. In our experiments, we use n_{boot} and n_{run} a few hundreds.